DESTRUCTION OF NITROGEN OXIDES USING A DIELECTRIC BARRIER DISCHARGE PLASMA REACTOR

By

PATRICK HARRY LYTLE

Bachelor of Arts

Hastings College

Hastings, Nebraska

1996

Submitted to the Faculty of the
Graduate College of the
Oklahoma State University
in partial fulfillment of
the requirements for
the Degree of
MASTER OF SCIENCE
May, 1998

DESTRUCTION OF NITROGEN OXIDES USING A

DIELECTRIC BARRIER DISCHARGE

PLASMA REACTOR

Thesis Approved:

Thesis Adviser

Dean of the Graduate College

PREFACE

This thesis was conducted to better evaluate the commercial viability of a dielectric barrier discharge (DBD) plasma reactor in the destruction of oxides of nitrogen (NO_x), a common by-product of internal combustion engines. These compounds are United States Environmental Protection Agency (EPA) criteria pollutants and contribute significantly to urban air pollution.

This report is organized into several sections. The introduction describes the NO_x problem and background of DBD plasma reactors and their application at Oklahoma State University and elsewhere. The theory section describes the mechanisms of plasma formation and reaction and various equations used to determine power consumption.

Following these sections, the procedure portion will describe the process variables examined and the materials and methods used to analyze the process. The results and discussion section will present findings and assess the advantages and disadvantages of the system and its variables. Then, the potential application of this type of reactor will be discussed in the engineering applications section. Finally, the overall success of the research and suggestions for further investigations will be presented in the summary section.

ACKNOWLEDGEMENTS

I wish to thank Dr. John Veenstra, my thesis advisor and friend, for his constant guidance and insight. No matter how flustered I became, he managed to find a way to solve the problem every time. Despite a busy schedule, he always found time to help me accomplish my goals.

Dr. Greg Wilber and Dr. Arland Johannes (A.J.), my other committee members, have also provided assistance without hesitation on numerous occasions. This support is greatly appreciated.

I also wish to extend my deepest gratitude to numerous other persons at Oklahoma State University and elsewhere. In particular, Dr. Thomas Gedra, of the School of Electrical and Computer Engineering, was an invaluable source of information and equipment for this research. Mark Christensen, an instructor in the Automotive Technology Department of Southeast Community College, Milford, Nebraska, provided important automobile system information. Other OSU faculty and staff, from Physics, Mechanical Engineering, Chemical Engineering, Biosystems Engineering, Biochemistry, and elsewhere all provided important information and materials.

Finally, my deepest and most sincere thanks must go to my wife, Michelle Lytle, and my parents, Carl and Marilyn Lytle. Their support has been both unfaltering and conditionless. My greatest hope is to be able to fulfill some of their dreams, as they have fulfilled scores of mine.

TABLE OF CONTENTS

Introduction **1**

The NO_x Problem 1
DBD Plasma Background 3
Previous Research at OSU 4
Previous Research Elsewhere 5

Theory **7**

Plasma Theory 7

Plasma Definition 7
Low-Temperature Plasmas 7
NOx Destruction Mechanisms 9
Descriptive Equations 11

Electrical Theory 12

RC Circuit Discussion 12
Power Consumption Equations 17

Procedure **18**

Materials 18

Reactor Construction 18
Power Supply 24
Electrical Measurements 24
Chemiluminescence Analyzer 26
Automobile Ignition Coil 26
Other Elements 27

Methods and Process Variables 28

Overview 28
Power Analysis 29
Gap Width 29
Reynolds Number Analysis 30

Destruction Efficiency Data 30
Humidity 31
Reactor Voltage 31
Residence Time 32
Statistical Analysis 32
Ozone Production 32
Extended Operation 33
Ignition Coil as Power Supply 33

Results and Discussion 34

General Comments 34
Power Analysis Results 34
Gap Width Comparison Results 43
Reynolds Number Results 44
Destruction Efficiency Results 45
Humidity Variation Analysis 45
Reactor Voltage Analysis 47
Residence Time and Frequency Analysis 48
Statistical Analysis 51
Summary of Operating Costs and Removal Rates 52
Ozone Production 54
Extended Operation 55
Ignition Coil as a Power Supply 56

Engineering Applications 57

Conclusions and Recommendations 59

References 62

Appendix A: Plasma Reactor Volume, Gap Width, and Capacitance Comparisons 65

Appendix B: Apparent Primary Power Plots for Reactor A and Reactor B 67

Appendix C: Power Curve Data 69

Appendix D: Reynolds Number Calculations 80

Appendix E: Destruction Efficiency Data.....82

Appendix F: Ozone Titration Data 85

LIST OF FIGURES

Figure 1: Simplified schematic of DBD reactor 3

Figure 2: Low-temperature plasma impact types 8

Figure 3: Chemical equilibrium for air at 1 atm 10

Figure 4: Voltage versus current in a capacitor 13

Figure 5: DBD reactor cross-section 14

Figure 6: Complex impedance diagram 15

Figure 7: Outer dielectric position 21

Figure 8: Reactor A profile 22

Figure 9: Reactor B profile 23

Figure 10: Reactor B bottom view, with and without endcap 23

Figure 11: Electrical schematic 25

Figure 12: Gas flow schematic 27

Figure 13: Apparent power plot versus primary voltage, Reactor A 35

Figure 14: Apparent power plot versus primary voltage, Reactor B 35

Figure 15: Transformer gain versus primary voltage for Reactor A data 36

Figure 16: Transformer gain versus primary voltage for Reactor B data 37

Figure 17: Typical voltage and current phase relationship 37

Figure 18: Real power versus secondary voltage for Reactor A 39

Figure 19: Real power versus secondary voltage for Reactor B 40

Figure 20: Voltage and current CRO traces at plasma-forming voltages 41

Figure 21: Voltage trace at plasma-forming voltages 41

Figure 22: Current trace at plasma-forming voltages 42

Figure 23: Effects of concentration and humidity on removal efficiency 45

Figure 24: Destruction efficiency versus reactor voltage plot 47

Figure 25: Removal efficiencies versus frequency for three flowrates 49

Figure 26: Removal efficiency versus cyclical residence time 50

Figure 27: Effluent temperature versus time 55

INTRODUCTION

> Modern man's capacity for destruction is quixotic evidence of humanity's capacity for reconstruction. The powerful technological agents we have unleashed against the environment include many of the agents we require for its reconstruction.
>
> George F. Will,
> Statecraft as Soulcraft: What Government Does

The NO_x Problem

Internal combustion engines produce a variety of unwanted by-products. These include carbon monoxide, hydrocarbons, ozone, and oxides of nitrogen. NO_x compounds specifically contribute to a wide variety of problems, from smog to acid rain. The Environmental Protection Agency reports that an average passenger car emits 1.5 grams per mile of nitrogen oxides (EPA 1997). In 1994, the United States alone released over 23,000 tons of NO_x, with mobile sources accounting for nearly 45 percent of that total (World Almanac 1997). The EPA has identified NO_x as one of six "criteria pollutants," and has established a threshold concentration (primary standard of 0.053 parts per million, annual arithmetic mean) above which adverse effects on human health may occur (EPA 1990). This concentration threshold is part of the National Ambient Air Quality Standards (NAAQS).

The use of catalytic converters to reduce NO_x to nitrogen and oxygen has been found to remove up to 90 percent of nitrogen oxides, depending upon operating conditions (Schäfer and van Basshuysen 1995). Unfortunately, these converters suffer from a number of drawbacks, including fouling from contaminants and poor cold-startup performance. Additionally, these systems are relatively expensive and produce backpressure in the exhaust system, which reduces fuel economy (Chaikin 1992). While

recent developments in converter technology have improved cold-start performance by pre-heating the catalyst, this modification may actually *increase* NO_x production (Comello 1996).

Clearly, room for an alternative treatment method remains. As discussed in the subsequent sections, dielectric barrier discharge (DBD) plasma reactors have been shown to remove NO_x compounds. In addition, research at OSU has indicated these reactors may cause hydrocarbon decomposition (Manning 1993). This indicates the potential of DBD reactors as an emission treatment technology.

The United States Patent Office has approved patents for a number of concepts and devices designed to reduce automobile emissions of hydrocarbons, oxides of nitrogen, and carbon monoxide. A patent approved in 1965 describes a concept of treating cool exhaust mixtures (not efficiently converted by traditional catalysts) with a silent electrical discharge (Specht 1961). This concept was further developed in a patent approved in 1971 (Newbold 1970). The application includes a diagram of a plasma-producing reaction chamber powered by the automobile's 12-volt battery, an invertor, transformer, and rectifier combination. More detailed patents (utilizing dielectric discharges to destroy NO_x and other compounds) were issued in 1994 and 1995 (Rich 1991, Rich et al. 1994). These applications describe a typical reaction chamber, power supply, and even give destruction efficiency results from a Cummins L-10 diesel engine. These patent applications indicate DBD discharge plasmas have a technical background and applicability to automobile exhaust.

DBD Plasma Background

DBD reactors consist of electrodes separated by one or more dielectric layers. As an AC high voltage is applied across these electrodes, an intense electric field is produced. This technology was first introduced by Siemens in the 1850's to produce ozone (Penetrante and Schultheis 1993). A simplified schematic of such a reactor is shown in Figure 1.

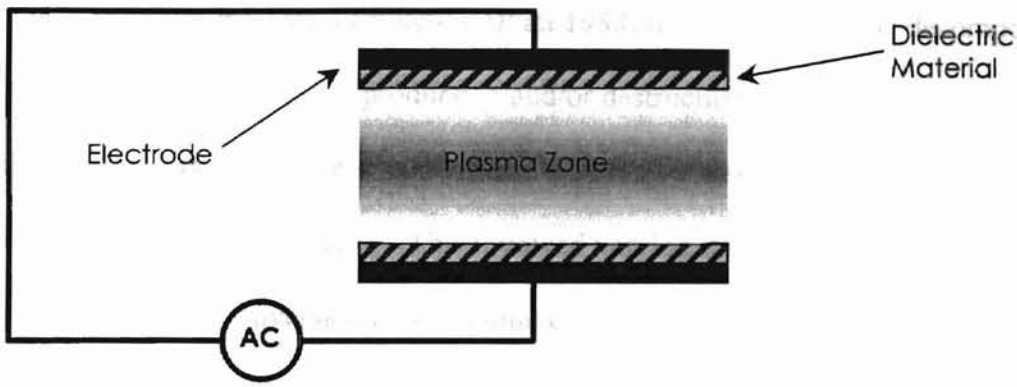

Figure 1: Simplified schematic of DBD reactor

These reactors are often termed "silent electrical discharge" reactors, as the dielectrics prevent any arcing between the electrodes. Silent discharge reactors are also characterized by operation at pressures of around one atmosphere (Glockler and Lind 1939).

DBD reactors have been used for various purposes in chemical processing and, more recently, in environmental remediation applications (Rosocha et al. 1993). The efficacy of the process depends upon a number of factors, including destruction efficiency, electrical stability, structural durability, and operating costs. These factors and others have been examined in various research projects, both at Oklahoma State University and elsewhere.

Previous Research at OSU

Plasma reactors have been the subject of graduate research at OSU since the late 1980's. This research has been conducted by students of Dr. Arland Johannes and Dr. John Veenstra, professors of Chemical Engineering and Civil and Environmental Engineering, respectively. In general, these investigations have centered on the destruction of organic or inorganic pollutants. Over ten theses have been presented on topics ranging from methane destruction (Piatt 1988) to hydrogen sulfide decomposition (Desai 1992). Specifically, the production and/or destruction of oxides of nitrogen have been studied previously by three students at OSU. These researchers all concentrated heavily upon "tuning" the reactor. This involved varying the frequency of the input voltage to maximize conversion or to minimize power consumption.

S.B. Robinowitz studied the variables that affect the rate of NO_x production in a DBD plasma reactor. His research concluded NO_x production to be directly proportional to input power, inversely proportional to flowrate, and maximized at 35% humidity. He also performed experiments in NO_x destruction. Percent destruction was determined to be a function of flowrate, with a maximum destruction level of 99.33% at around 100 ml/min (Robinowitz 1992).

G.S. Sidhu also examined production and destruction of nitrogen oxides. Sidhu determined the formation of nitrogen oxides is directly proportional to residence time. Humidity seemed to have little effect upon NO_x formation at lower residence times, but did increase production rates at longer residence times (Sidhu 1995).

Notes from M. Falk's research in NO destruction indicate increased humidity levels tend to increase percent destruction. He also determined decreasing the residence

time by a factor of two only minimally decreased the destruction efficiency. A maximum destruction level to 8 ppm residual was observed, but Falk was unable to determine if this was a characteristic of the reactor itself or the NO_x analyzer (Falk 1994).

Previous Research Elsewhere

Researchers at Los Alamos National Laboratory have used DBD plasma reactors to treat hazardous organic pollutants, including trichloroethylene (TCE) and carbon tetrachloride (Rosocha et al. 1993). They have applied this technology to a number of actual waste sites in field-scale tests (Neidorf 1996). Furthermore, they have indicated the potential of such a system for treating NO_x and sulfur oxides (SO_x), as well as auto emissions (Rosocha et al. 1995).

A number of research teams in Japan have applied DBD plasma technology specifically in the area of auto emission treatment. One group studied simultaneous NO_x, CO_x, and SO_x removal in diesel engine exhaust with a DBD reactor (Fujii et al. 1993). This particular system included a diffuser which injected motor oil into the annular space of the reactor. The addition of the oil was determined to increase soot removal and to help generate a more uniform discharge plasma. A maximum NO_x removal rate of 69% was observed, along with a corresponding reduction in carbon and sulfur oxides and soot.

Another Japanese study concerned the removal of ammonia and NO_x in a gas stream (Chakrabarti et al. 1995). A number of process variables were examined, including residence time, applied waveform, and humidity. It was determined longer residence times gave rise to increased levels of nitrous oxide (N_2O), an undesired byproduct. A 250 hertz positive pulsed square wave was found to increase destruction

efficiency at all humidity levels. For both 60 hertz and 18 kilohertz sine waves, destruction efficiency increased with humidity. Humidity was increased by applying a wet filter paper to the inner surface of the outer electrode. This configuration was found to be a positive way to hasten the onset of a plasma formation, but unfortunately caused arcing at higher voltages and longer residence times.

THEORY

> The lightning flashes through my skull; mine eyeballs ache and ache; my whole beaten brain seems as beheaded, and rolling on some stunning ground.
>
> Captain Ahab, in Herman Melville's Moby-Dick

Plasma Theory

Plasma Definition: Efforts to find an overarching definition for the word "plasma" have met with considerable challenges, due to the wide variety of production methods, physical conditions, and desired uses for different plasma types. The unique characteristics of plasmas have lent to them being considered a fourth state of matter (Serway 1990). The term was first used by Irving Langmuir in 1926 to describe the inner region of an electrical discharge. This definition was later expanded to describe "a state of matter in which a significant number of the atoms and/or molecules are electrically charged or ionized." (Boenig 1982)

In actuality, the plasma state is far more common throughout the universe than the more familiar forms of solid, liquid, and gas. It can be found inside stars, within interstellar gases, and commonly on earth by lightning bolts. These three examples also indicate the three methods by which plasmas are formed: thermally (stellar interiors), radiation-induced (interstellar gases), and electrically (lightning).

Low-Temperature Plasmas: As may be expected, low-temperature or non-thermal plasmas are formed by the latter two mechanisms mentioned above. The required ionization is achieved by effectively raising the temperature, or speed, of the electrons in the gas while allowing the heavier particles (nuclei) to remain at near-ambient temperatures. By applying a flux of photons (radiation-induced) or an alternating high

voltage (electrically-induced), the electrons are freed from their nuclei and the gas becomes a conductor (Coffman and Browne 1965). Once freed, these electrons are able to interact with atomic nuclei by a number of methods. There are four principle methods of interaction, characterized by the type of impact the electron makes with the other particles (Glockler and Lind 1939).

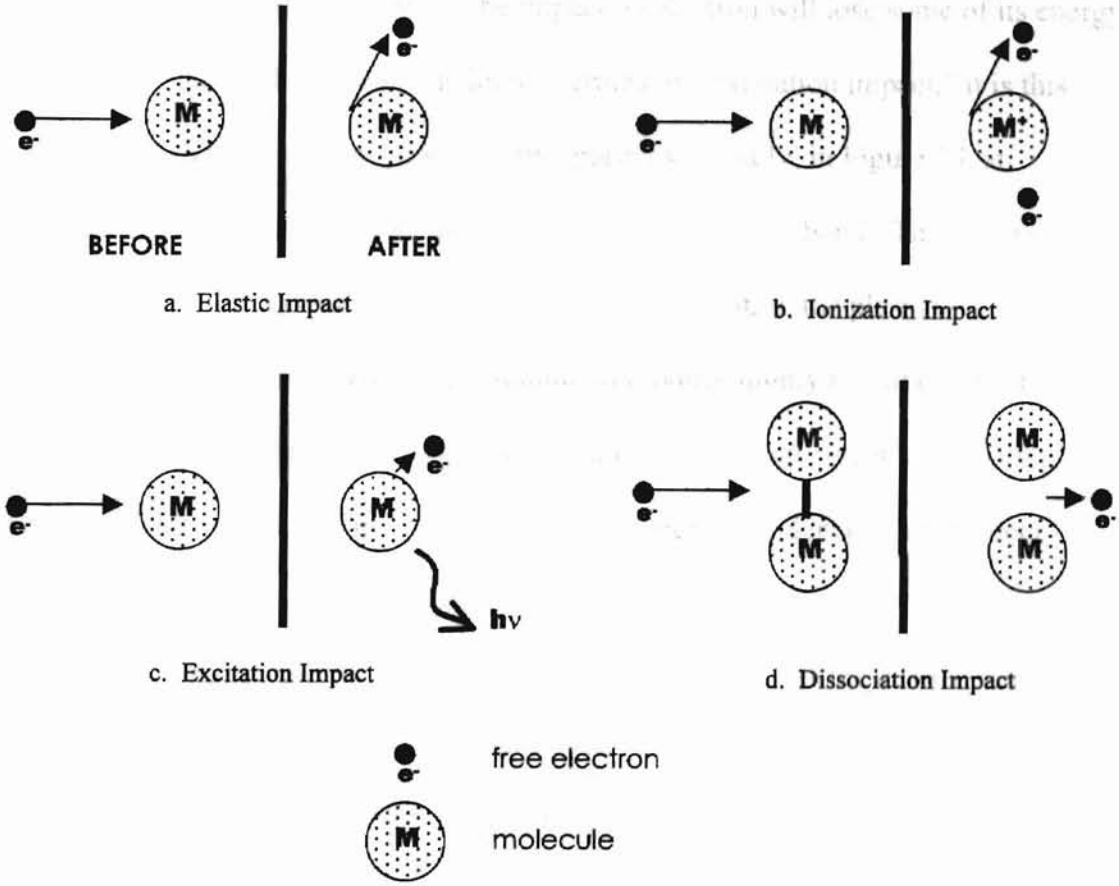

a. Elastic Impact

b. Ionization Impact

c. Excitation Impact

d. Dissociation Impact

Figure 2: Low-temperature plasma impact types

Figure 2a represents an electron colliding with an atomic nucleus and essentially bouncing off. The large difference in masses of the two particles makes this scenario relatively probable. In 2b, the electron collides with the nucleus, knocks another electron loose, losing a large portion of its energy in the process. This interaction helps produce a

"flood" of electrons, which combine to produce a large number of the other three interactions, as well as a positively charged molecule (radical) more likely to interact with other species. Figure 2c shows the consequence of an electron striking a nucleus, exciting an inner shell electron to a higher valence level. This excited electron will eventually return to its original position and give off a photon with energy equal to the difference of the two valence levels. The impacting electron will lose some of its energy and continue to travel through the medium. Termed an "excitation impact," it is this interaction which produces the glow of active plasmas. Finally, in Figure 2d, an incoming electron supplies enough energy to break a molecular bond. This allows the dissociated molecules to react with other species present within the plasma.

With these four mechanisms combining to produce highly reactive radicals, various chemical reactions take place which, among other things, break down complex and otherwise stable substances. By varying the humidity, residence time, influent concentration, and energy supplied to the reactor, the operator may fine-tune the plasma. This minimizes the amount of unwanted reactions and maximizes the desired reactions.

NO_x Destruction Mechanisms: For the purpose of this research, possible reaction pathways for the conversion of NO and NO_2 to N_2 are of particular interest. These have been documented in various sources (Glockler and Lind 1939, McTaggart 1967, Penetrante 1993).

$$2NO_2 + 2e\ (fast) \rightarrow N_2 + 2O_2 + 2e\ (slow)$$
$$NO_2 + e\ (fast) \rightarrow NO + O + e\ (slow)$$
$$2NO_2 + O_2 \rightarrow 2NO_2$$
$$N + NO_2 \rightarrow 2NO$$
$$N + NO_2 \rightarrow N_2 + O_2$$
$$N + NO \rightarrow N_2 + O$$

As previously discussed, these reactors generally produce ozone (O_3) to varying degrees as well. Its presence will provide for the following potential reactions.

$$O_3 + NO \rightarrow NO_2 + O_2$$
$$N + O_3 \rightarrow NO + O_2$$

The specific conditions that produce these destruction reactions are extremely difficult to quantify and will not be discussed here. However, general trends in the equilibrium between oxygen, nitrogen, and nitrogen oxides may be found and plotted in a graph of concentration versus temperature. Such a graph for air (79% nitrogen 21% oxygen) at one atmosphere pressure is presented in Figure 3.

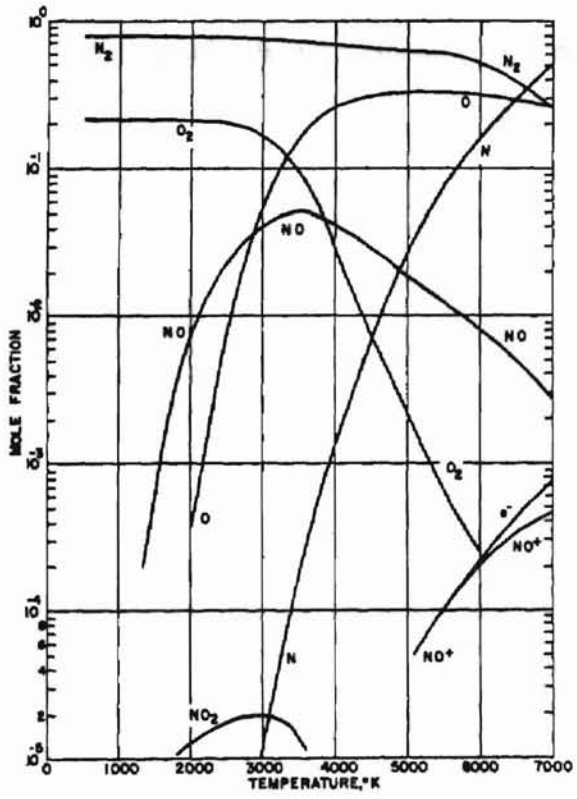

Figure 3: Chemical equilibrium for air at one atm (Baddour and Timmins 1967)

By adjusting the applied voltage, the theoretical (electron) temperature of the gas may be adjusted as well. If the effluent concentration of any of the species shown in Figure 3 is known, the approximate theoretical temperature of the gas may be determined.

Descriptive Equations: By finding the voltage across the annulus of the reactor, a maximum velocity for the freed electrons can be calculated. The potential energy for a point charge within an electric potential is written

$$U = Vq \qquad [1]$$

where: U=energy of particle (Joules)
V=applied voltage (volts)
q=particle charge (coulombs).

To determine the electron's velocity, substitute the kinetic energy equation for E [2] and solve for velocity.

$$U = \frac{1}{2}Mv^2 \qquad [2]$$

where: M=particle mass (kg)
v=velocity (m/sec).

$$v = \sqrt{\frac{2Vq}{M}} \qquad [3]$$

The theoretical temperature of the electrons may be determined if their velocity is known, using the following equation

$$T = \frac{mv^2}{3R} \qquad [4]$$

where: T=particle temperature (K)
m=particle molar mass (kg/mole)
R=Universal Gas Constant ($kg*m^2/(sec^2*K*mole)$.

Substituting equation [3] into [4] and inserting known values for q ($1.6*10^{-19}$ coulomb), m ($5.48*10^{-7}$ kg/mole), M ($9.11*10^{-31}$ kg), and R (8.34 J/K*mole), the following relationship between maximum electron temperature and applied voltage is established.

$$T = 7720(V) \qquad [5]$$

While this equation indicates *extremely* high electron temperatures may be achieved with relatively ordinary voltages, it is important to remember that this represents the *maximum* velocity (temperature) an electron may achieve. In actuality, the majority of electrons will not be accelerated across the entire gap due to collisions and their initial position within the gas. However, the equation does serve to indicate the important role the accelerating voltage plays in increasing the theoretical electron temperature.

Electrical Theory

RC Circuit Discussion: In order to understand the electrical properties of DBD plasma reactors, a number of alternating current (AC) circuit characteristics must be discussed. These include the phase relationship between voltage and current, the theoretical capacitance of the reactor, and the impedance of capacitors in general.

Circuit theory indicates that, in an AC circuit, the current flowing through a capacitor *leads* the voltage by 90 degrees (Simpson 1987). This is explained by the equation which relates current to voltage

$$i = C\frac{d}{dt}(V) \qquad [6]$$

where: I=current (amps)
C=capacitance (farads)
V=voltage (volts).

As commonly practiced, the voltage is represented by a cosine function of the form

$$V = V_o \cos(\omega t) \qquad [7]$$

where: V_o=amplitude of voltage (volts)
ω=angular frequency (-)

The corresponding current function is determined by substituting equation [6] into [7]

$$i = -V_o C \sin(\omega t) \qquad [8]$$

Plotting these functions would produce graphs of the form shown in Figure 4.

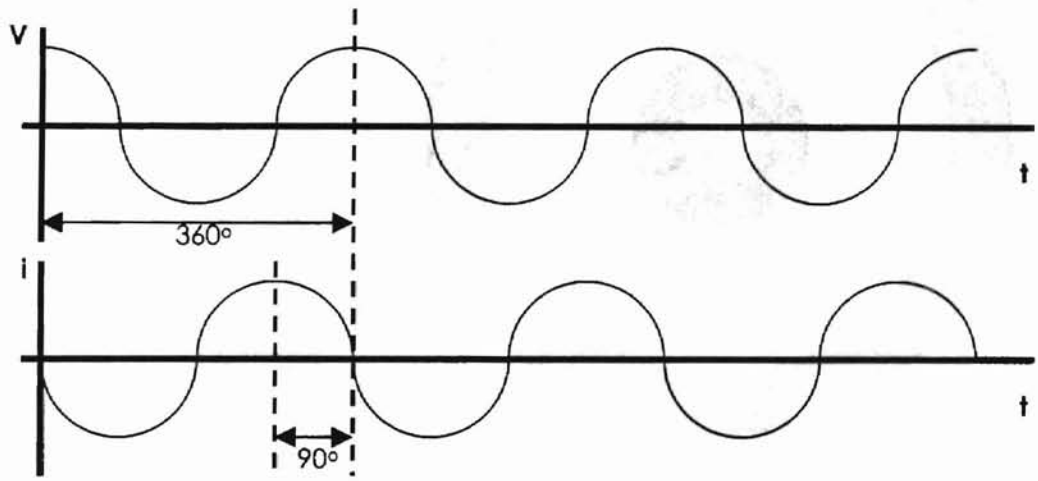

Figure 4: Voltage versus current in a capacitor

From this graph, the phase relationship between voltage and current is apparent.

Prior to formation of a plasma in its annulus, the DBD plasma reactors used at OSU are essentially examples of cylindrical capacitors. As such, they have a theoretical capacitance equal to

$$C = \frac{l}{2k \ln(\frac{a}{b})} \quad [9]$$

where: k=permittivity constant ($N*m^2/C^2$)
a=inner radius (m)
b=outer radius (m)
l=length (m).

However, the presence of dielectric material between the inner and outer electrodes produces different k values between the inner and outer radius. Figure 5 shows a cross section of such a reactor, with dielectrics inserted.

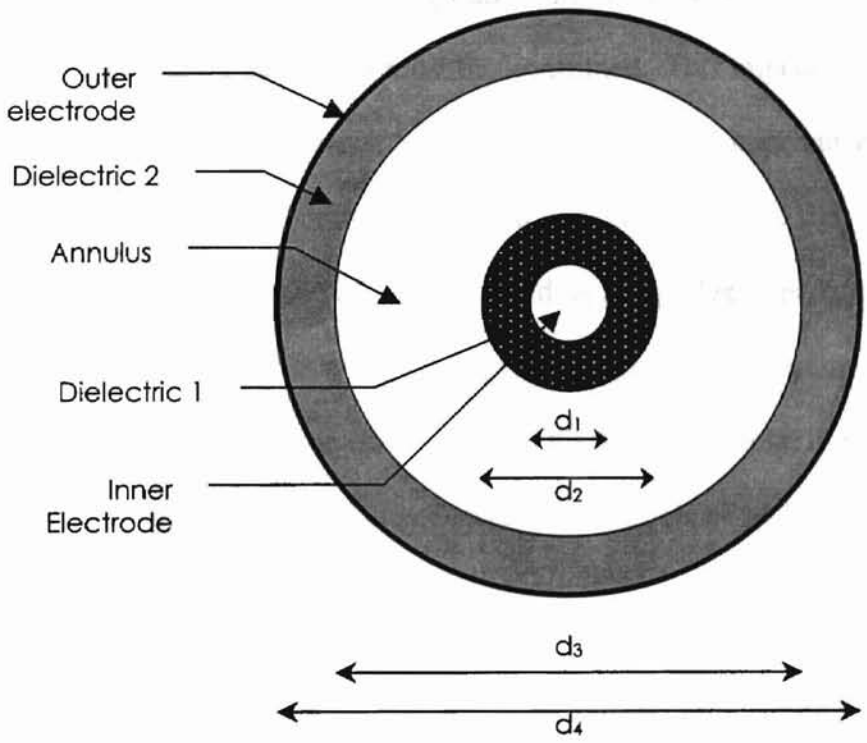

Figure 5: DBD reactor cross-section

The addition of the dielectrics creates a series of concentric cylindrical capacitors. Therefore, the capacitance of each pair of cylinders must be calculated individually,

accounting for the material in between them (either dielectric 2, air, or dielectric 1). Circuit theory defines the capacitance of a series of capacitors as

$$\frac{1}{C_{total}} = \frac{1}{C_1} + \frac{1}{C_2} + \frac{1}{C_3} \qquad [10]$$

By knowing the length of the reactor, the diameters d_1, d_2, d_3, and d_4 from Figure 5, and the dielectric constants of dielectrics 1 and 2, the total capacitance of the reactor may be calculated.

In order to calculate the power consumption of the circuit (to be discussed later in this chapter), the impedance of the reactor must be determined. This impedance, like resistance, is expressed in ohms. However, unlike resistors, the total impedance of a series of impedances is not the sum of their individual impedances. Since the current leads the voltage in capacitors, the impedance is plotted on a complex impedance diagram, with real voltage (such as that across a resistor) plotted on the horizontal and capacitive impedance plotted along the vertical axis. This produces a total impedance equal to the *vector sum* of the individual impedances. An example of such a plot is shown in Figure 6.

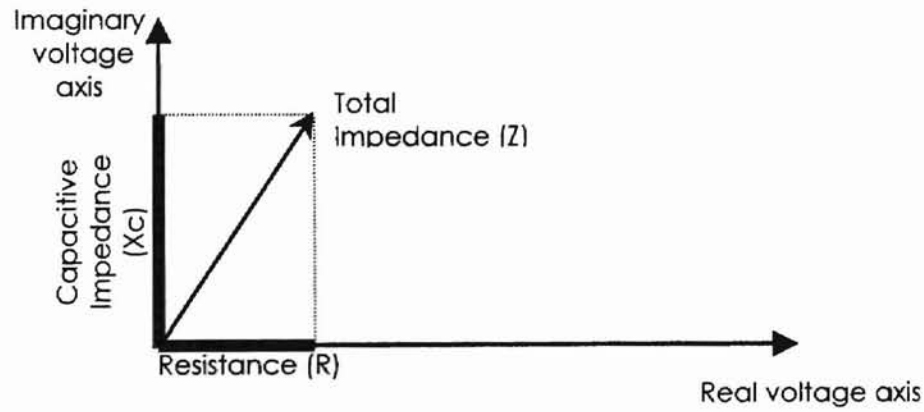

Figure 6: Complex impedance diagram

As previously mentioned, the net impedance of the circuit is the vector sum of the two impedances. Solving for Z,

$$Z = \sqrt{R^2 + X_c^{\,2}} \qquad [11]$$

where: Z=net impedance (ohms)
X_c=capacitive impedance (ohms).

However, it is still necessary to define X_c, the capacitive impedance.

$$X_c = \frac{1}{j\omega C} \qquad [12]$$

where: j=complex integer
ω=angular frequency (=2πf).

The presence of the complex j simply takes into account the phase relationship between current and voltage in a capacitor. The magnitude of X_c depends only on ω and C. From this, it becomes apparent that the impedance is inversely proportional to frequency and capacitance. Hence, the greater the capacitance of the reactor, the lower its impedance.

Previous research at OSU has indicated the need for considering the internal impedance of the transformer used to power the circuit (the complete circuit will be discussed in the following chapter). This led to consideration of a circuit containing three types of impedances and the necessity of finding the resonant frequency of the circuit, where the inductive impedance was equal in magnitude to the capacitive impedance. However, for an open circuited transformer, the secondary winding may be considered a "perfect" voltage source (Gedra 1997). This allows the inductive impedance portion to be removed from consideration. Secondary currents measured by past researchers (Krishnamoorthy 1996) and in this study (refer to Results and Discussion chapter) have

all been in the 0-500 microamp (μA) range. This produces an essentially "open" secondary circuit. Therefore, "tuning" of the reactor (maximizing input power by varying the frequency) and the theory of RLC series circuits is not discussed herein.

Power Consumption Equations: Previous researchers at OSU have also endeavored to determine the power required for the DBD plasma reactor. Various methods have been used to determine this variable. Unfortunately, most have relied upon measuring the current and voltage supplied to the primary side of the transformer. These methods have generally not taken into account the phase angle relationship of current and voltage, which drastically affects the *real* power used by the circuit, as shown below.

$$P_{app} = IV \qquad [13]$$

where: P_{app}=apparent power (watts)

$$P_{real} = IV\cos(\phi) \qquad [14]$$

where: P_{real}=real power (watts)
ϕ=phase angle (degrees)

Simply stated, "real power" is the power users pay for. As evidenced by equation [14], a voltage and current out of phase by 90 degrees will produce a real power consumption of 0.00 watts. In order to find the real power used by the reactor, it is necessary to use a watt-hour meter or measure the phase angle between voltage and current.

The second problem with earlier methods of measuring power consumption at OSU was the location at which that power was measured. To get a true idea of how much it costs to operate a DBD plasma reactor, the power required by the *reactor itself* should be determined, not the power required by the transformer used to "step-up" the voltage for the reactor.

PROCEDURE

So many worlds, so much to do,
So little done, such things to be.

Lord Tennyson, In Memoriam

Materials

Reactor construction: In the past, plasma reactors at OSU were typically constructed of a blown-glass vessel. These reactors were initially setup with various configurations of wire mesh, wire wrappings, and a conducting silver paint for electrodes. Unfortunately, these configurations were less likely to produce a uniform plasma in the reactor annulus and prevented physical viewing of a plasma glow (Parker 1996). By switching to liquid electrodes (utilizing solutions of copper sulfate or ethylene glycol), researchers were able to overcome these limitations. However, both the use of relatively fragile glass reactors and the advent of liquid electrodes severely limited the potential operating environments of the reactors. Besides the consideration of plasma uniformity, the chief drawback of metal electrodes was the presence of an exposed high-voltage electrode (Parker 1996). This safety issue has been addressed by grounding the outer electrode, which confines the presence of high voltages to within the reactor vessel.

In order to produce a reactor which was both rugged and safe, a number of materials were examined for use as electrodes and dielectrics. In addition, the theoretical capacitances, annular volumes, and gap widths of several reactors used previously at OSU were calculated to ensure any new reactors had characteristics similar to previous ones. These comparisons are presented in Appendix A.

To aid in the fabrication of cylindrical reactors, various sizes and wall thicknesses of metal pipes were considered. For inner electrodes, a number of gauges of wire, along

with flexible copper tubing were examined to produce the correct capacitance and gap width.

Dielectric materials must be flexible, resistant to chemical attack, and have a high dielectric strength to prevent arcing between the electrodes. Teflon (tetrafluoroethylene) was selected as a suitable candidate for the dielectric. The pertinent characteristics of Teflon are presented in Table 1.

Characteristic	Value	Source
Dielectric Strength (breakdown voltage)	60 MV/m	Serway 1990
Dielectric Constant	2.1	Serway 1990
Maximum Operating Temperatures	>285 °C (dielectric stability) 340 to °360 C (melting pt)	NASA 1992
Molding qualities	excellent	Von Hippel 1954
Dissipation factor (charge loss)	<0.0002	Von Hippel 1954
Chemical resistance	very high	Atkins and Beran 1995

Table 1: Teflon properties

This combination of properties makes Teflon an ideal material for lining the reactor and to serve as the dielectrics between the electrodes. Two reactors were constructed with nearly equal theoretical capacitances, one (Reactor B) with twice the gap width of the other (Reactor A). An overview of all the materials used for reactor fabrication is presented in Table 2.

Component	Size	Thickness	Notes
Reactor A, inner electrode	9 gauge wire 0.29 cm OD	N/A	
Reactor A, inner dielectric	0.30 cm ID Teflon	0.05 cm	
Reactor A, outer dielectric	Teflon sheet	0.16 cm	requires bonding
Reactor A, outer electrode	¾" Schedule 40 2.06 cm ID	0.29 cm	
Reactor A, endcaps	#1 stopper	N/A	neoprene
Reactor B, inner electrode	3/8" copper tubing 0.95 cm OD	N/A	
Reactor B, inner dielectric	0.95 cm ID Teflon	0.09 cm	
Reactor B, outer dielectric	Teflon sheet	0.16 cm	requires bonding
Reactor B, outer electrode	2" Schedule 160 4.21 cm ID	0.87 cm	
Reactor B, endcaps	#8 stopper	N/A	neoprene

Table 2: Reactor material overview

The outer dielectrics were fabricated from a sheet of Teflon material. All Teflon materials were purchased from COPE Plastics, Inc. of Oklahoma City, Oklahoma. To provide a continuous lining within the outer electrode, the sheet was sized and then rolled to contact the pipe's interior as shown in Figure 7. The overlap shown in the picture was added as a safety precaution to prevent arcing. While this produced a slight variation in the actual capacitance and annular volume, the net effect was negligible (as evidenced by the comparison of calculated and measured capacitances in Table 4). The surface of the dielectric which was in contact with the outer electrode had to be etched and bonded to the surface (using Chemgrip® bonding kit), since Teflon's extreme resistance to chemical interaction prevented normal adhesives from holding.

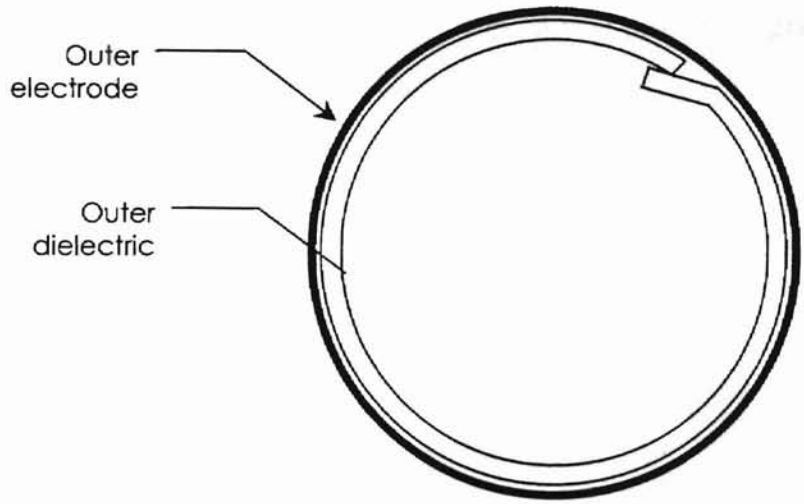

Figure 7: Outer dielectric position

After the dielectrics were attached to the electrodes, the final details of reactor construction were completed. One-quarter inch plastic hose barbs were added on opposite sides to supply influent and effluent points to the reactor, and the ends of the reactors were sealed with non-reactive neoprene rubber stoppers. The overall characteristics of the reactors are summarized in Table 3. The annular volume was calculated based upon physical measurements with calipers.

Parameter	Reactor A	Reactor B
Effective Length	28 cm	21 cm
Gap width	0.67 cm	1.38 cm
Annular volume	62.9 cm^3	228.5 cm^3

Table 3: Reactor characteristics summary

The following pictures show the completed reactors. Each is shown in a side view and Reactor B is shown with an endcap in place and then removed to indicate a

cross-section. Each reactor was wrapped with Teflon to prevent possible degradation of the outer electrode and to help hold the outer electrode's connecting wire in contact with the cylinder's surface.

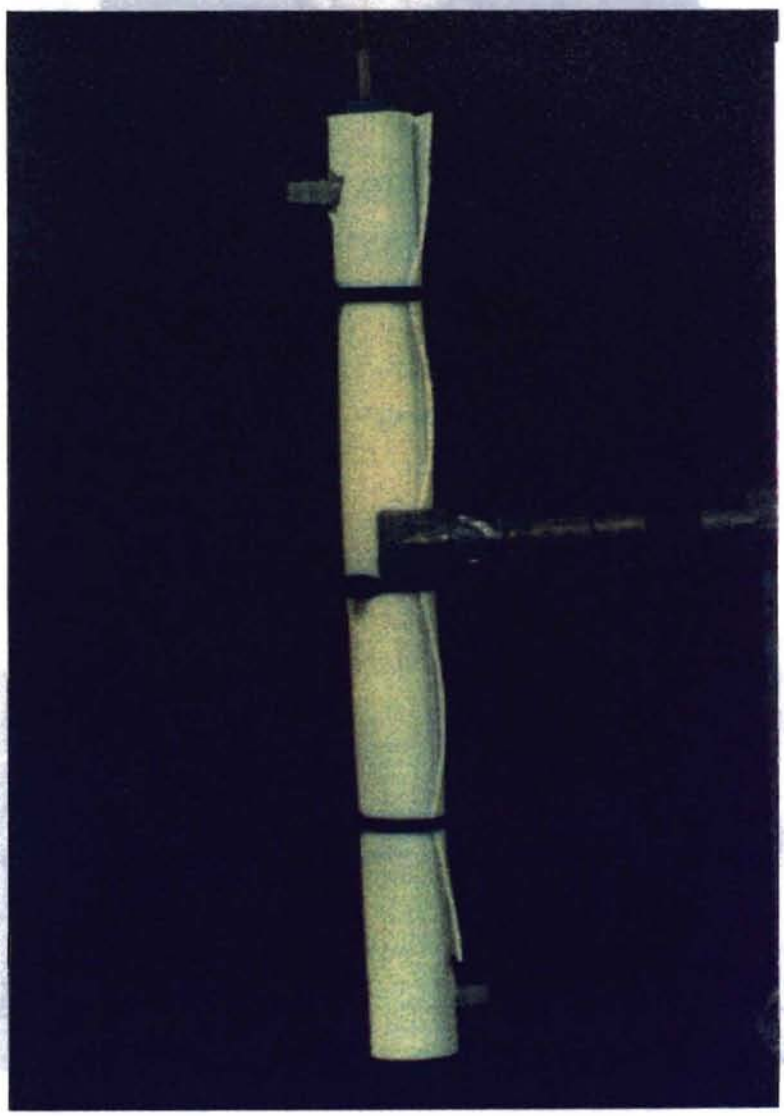

Figure 8: Reactor A profile

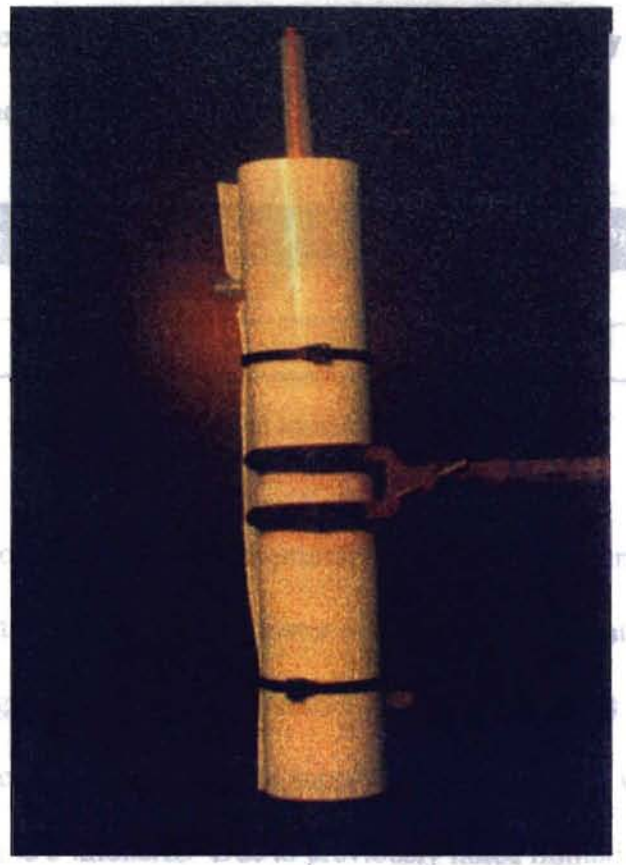

Figure 9: Reactor B profile

Figure 10: Reactor B bottom view, with and without endcap

In addition, the capacitance of each completed reactor was measured using a Hewlett Packard Model 4261A LCR meter. The results of these measurements are summarized in Table 4. Measured values were quite similar to theoretical values,

considering many factors (humidity, surface irregularities, proximity to other conductors, etc.) may influence actual capacitances.

	Theoretical Capacitance	Measured Capacitance
Reactor A	9.97 picofarads (pF)	13 pF
Reactor B	9.84 pF	18 pF

Table 4: Reactor capacitance comparison

Power supply: The voltage source for the primary side of the transformer was a California Instruments Model 161T AC power source, with an output power rating of 160 VA and output voltage range of 0-120 volts root mean squared (rms). This supply has a built in oscillator (Model 800T) capable of supplying sinusoidal AC voltages from a frequency of 40 hertz to 5 kilohertz. Due to previously noted limitations of the power supply at frequencies below 100 hertz (Tsai 1991, Parker 1996), the oscillator was only used at frequencies of 120 hertz and greater.

The transformer used in this experiment is typically used in neon sign power supplies. This "gaseous tube" type transformer was a Franceformer Model 15060P, with a maximum input voltage of 120 V at 60 hertz.

Electrical measurements: A number of multimeters were used to measure voltage and current at various places in the circuit. These locations are shown in Figure 11. These meters were Radio Shack Model 22-163. The high voltage probe (measured voltage = 1/1,000 actual voltage) across the transformer secondary was manufactured by Fluke, Model 80K-40. As mentioned in a previous thesis (Parker 1996), these voltage probes are rated at 60 hertz *only*, and are not be reliable at other frequencies.

Other measurements on the secondary side were taken using a Tektronix Model 2235 cathode-ray oscilloscope (CRO) and Tektronix P6015A high voltage probe (operable at frequencies from DC to 75 MHz). Both channels of the oscilloscope were utilized to measure reactor voltage and secondary current. This secondary current was determined by measuring the voltage drop across a measuring resistor (1000 ohms). In addition, the phase difference between the two channels could be estimated, and the waveform could be examined to ascertain any variances due to plasma formation.

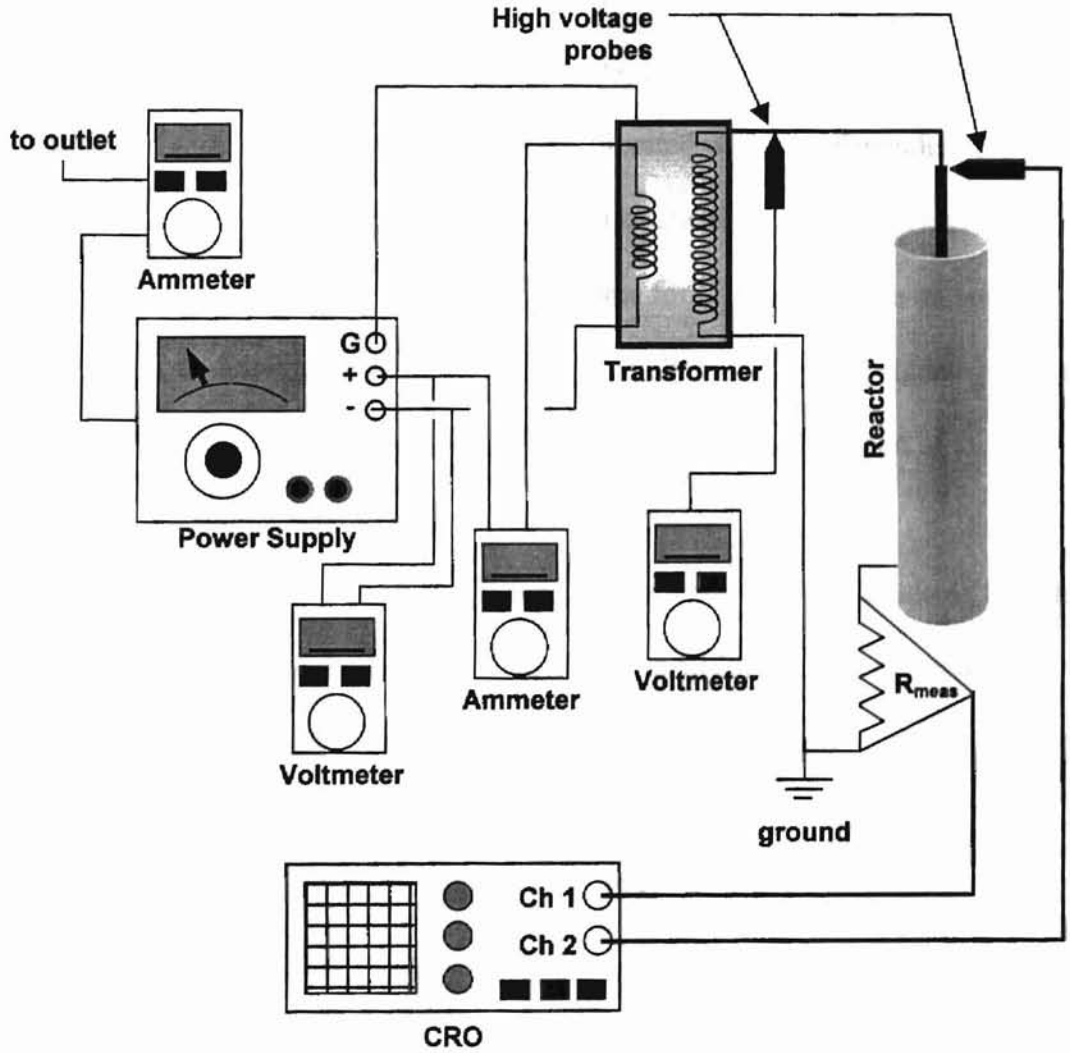

Figure 11: Electrical schematic

Chemiluminescence analyzer: In order to determine NO_x destruction by the reactor, it was necessary to measure the concentration of NO_x entering and leaving the reactor. A Thermo Electron Model 10A Chemiluminescence Analyzer, capable of online measurement of concentrations from 1 to 10,000 ppm was used. When operated in NO_x mode, the instrument first passes the gas through a converter which transforms all the NO_x into NO. The gas is then fed into a reaction chamber and reacts with ozone. This reaction produces light of a particular wavelength. A photomultiplier tube adjacent to the chamber measures the amount of light produced; this generates a current proportional to the NO_x concentration of the sample which is displayed on an analog dial in ppm. Prior to each group of experiments, the analyzer was calibrated with an independent NO_x certified standard ($[NO_x]$=479.6 ppm) from Praxair of Bethlehem, Pennsylvania.

Automobile ignition coil: One potential power source for DBD reactors is an ignition coil from a passenger automobile, which supplies a high voltage alternating signal. Since the coil is already present on all automobiles, it would simplify the adaptation of DBD reactors to treating auto exhaust.

The input to the coil of is an on-off type square wave with amplitude of 12 volts (supplied by the car's battery). This input is stepped up within the coil to voltages ranging from 10,000 to 50,000 volts. This signal is transferred to the spark plugs, causing them to fire. For an engine operating at 3,000 rpm, this corresponds to a frequency of approximately 50 hertz (Christensen 1997).

For this experiment, an ignition coil from an HEI (high-energy ignition) system was used. This type of coil is found in most 1988 to 1992 model General Motors

vehicles and produces a typical output voltage of 25,000 volts maximum (Christensen 1997).

Other elements: The method of gas blending and delivery to the NO_x analyzer is shown in Figure 12. The NO_x tank contained 1% NO_2 (10,000 ppm by mass) from Scott Specialty Gases of Houston, Texas, in a balance of air and the second tank contained the blending gas, which was dry grade breathing air. The flowrates of the NO_x and the blend were measured with two of four Manostat 150 mm flowmeters from Fisher Scientific, dependent upon the desired range of flowrates. These flowmeters allowed measurement of air phase flows from 1.7 to 24,400 ml/min.

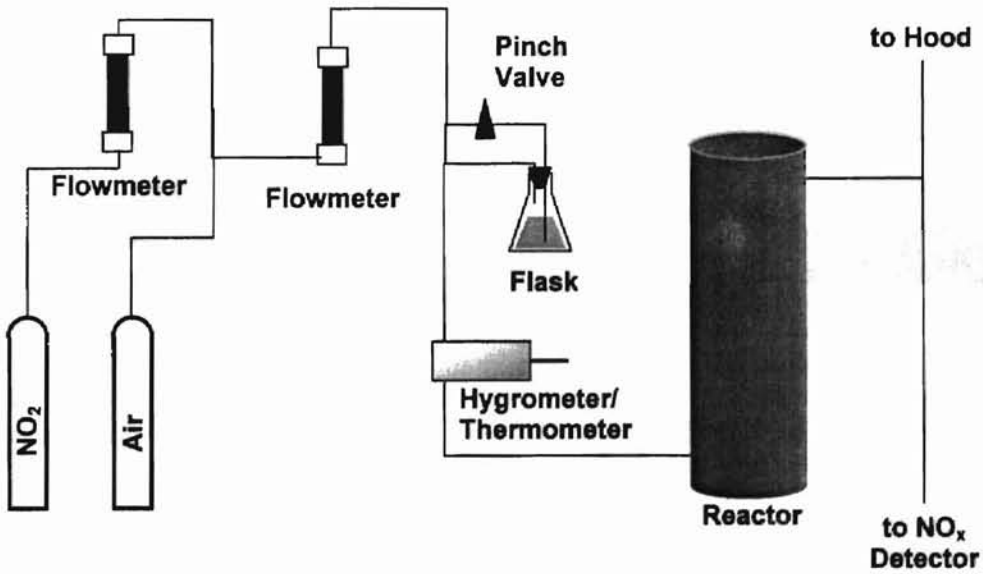

Figure 12: Gas flow schematic

A tee in the line with a pinch valve allowed a portion of the flow to pass through the headspace or below the water surface of a 500 ml Erlenmeyer flask filled with water. By adjusting the valve, various influent humidities could be attained. A Universal

Enterprises digital hygrometer/thermometer, model DTH1, measured the relative humidity of the gas entering the reactor and was later relocated to measure the effluent gas temperature. This meter is only reliable to about ± 5% relative humidity, but was used only to determine approximate humidity levels (low, mid, and high). Since all runs were conducted at essentially the same temperature, the relative humidity was also a good indicator of absolute humidity. All tubing was ¼ inch Tygon, unlined upstream of the reactor and Teflon lined downstream of the reactor to prevent ozone degradation.

Methods and Process Variables

Overview: The following table summarizes the process variables examined in this thesis. Each was selected to help demonstrate the commercial feasibility of DBD reactors. The following sections describe the procedure used to examine these variables in detail.

Variable	*Method of Analysis*	*Rationale*
Power consumption	CRO measurements of voltage, current, and phase angle estimation	Gives estimate of cost of operation and supply circuit requirements
Reynolds number	Mathematical calculation	Verifies laminar flow
Destruction efficiency	Measurement of NO_x concentrations of influent and effluent	Establishes overall effectiveness of DBD reactor
Residence time	Calculation of flowrate and reactor annular volume	Determines processing rate of reactor, affects costs of operation
Statistical analysis	Replication of experimental data sets	Gives an idea of reproducibility and reliability of process
Humidity	Passing influent through blending system	Relates destruction efficiency and influent humidity
Gap width	Reactor construction	Relates electrode separation and power consumption
Ozone production	Iodometric titrations	Estimates unwanted by-product formation rates
Extended operation	Electrode temperature measurement	Determines long-term thermal stability of unit
Ignition coil as power supply	Replace transformer with coil	Provides indication of applicability to auto exhaust

Table 5: Process variable overview

Power analysis: Figure 10 shows the circuit layout used to examine the power consumption characteristics of the DBD reactors. Previous researchers have referred to these power determinations as "non-destructive tests" (Tsai 1991).

The basic procedure for power consumption determination is described below:

1. Span gas (air) flow through the reactor was established and frequency was set on power supply.
2. Primary voltage was adjusted from 0 to approximately 110 volts in 5 volt increments.
3. Readings of wall current, primary current, secondary voltage, reactor voltage, secondary current, and secondary phase angle were taken for each primary voltage.
4. Primary voltage was increased until reactor voltage reaches 8,000 volts for Reactor A or 10,000 volts for Reactor B.
5. Frequency was adjusted, and steps 2-5 were repeated.

From this data, power consumption (both apparent and real) were plotted versus primary or secondary voltage. Since both current and voltage in the secondary were known, the experimental impedance of the reactor-measuring resistor combination was plotted as well. This impedance can be compared to the calculated impedance of the combination from LCR meter measurements. In addition, the gain of the transformer versus frequency may be plotted. To compare results to those of other researchers at OSU, plots of apparent primary power versus frequency may also be prepared. By examining the phase relationship and waveforms of the secondary voltage and current, the critical voltage of plasma formation was apparent.

Gap width: The two reactors were designed to have nearly the same capacitance (impedance), but Reactor B was designed with a gap width equal to twice that of Reactor A. This produces nearly identical electrical circuits, but different physical configurations.

The power requirements, plasma formation voltage, and treatment rate of the two reactors were then compared to determine the overall effect of increased gap width.

Reynolds number analysis: To determine whether laminar or turbulent flow exists in the reactors, the maximum flowrate and reactor dimensions were entered into the following equation (McCabe and Smith 1976) to calculate the highest Reynolds number likely in the system

$$N_R = \frac{4Q\rho}{\mu(D_O - D_I)\pi} \qquad [15]$$

where: Q=flowrate (m^3/sec)
ρ=density of liquid (kg/m^3) (air=1.23)
μ=viscosity of liquid ($N*s/m^2$) (air=$1.79*10^{-5}$)
D_O=outer diameter (m)
D_I=inner diameter (m).

While sources disagree on the exact boundary between laminar and turbulent flow, Reynolds numbers less than 2,000 may generally be considered laminar (Munson et al. 1994). If laminar flow is prevalent, the fluid velocity varies, based on proximity to the reactor's walls. If the flow scheme is primarily turbulent, the fluid velocity is relatively constant across the reactor, and various simplifying assumptions may be made when modeling the system.

Destruction efficiency: To quantify the amount of NO_x removed by the reactor, the following procedure was used:

1. The NO_x detector was started up and calibrated according to the procedures outlined in its manual.
2. NO_x and span gas flowrates were set to provide the correct residence time and concentration. Flows were allowed to stabilize (<2% variation ±).
3. The detector reading was allowed to stabilize (usually about 5 minutes elapsed time) and the influent concentration ($C_{o,I}$) was recorded.

4. The reactor was turned on by supplying the appropriate secondary voltage, and the effluent concentration (C_e) was monitored. After C_e stabilized, the value was recorded and power to the reactor was turned off.
5. To account for possible fluctuations in gas flows during the time of the run, the concentration was allowed to stabilize a third time, and the ending influent reading was taken and recorded as $C_{o,2}$.
6. The average of $C_{o,1}$ and $C_{o,2}$ was calculated and recorded as C_o.
7. Destruction efficiency was calculated using equation [16].
8. Steps 2 – 7 were repeated for varying influent concentrations.

$$X_d = \frac{C_o - C_e}{C_o}(100\%) \qquad [16]$$

Humidity: The presence of water vapor within the plasma has been found to significantly affect removal efficiencies and by-product formation rates (Chang et al. 1993). For this reason, destruction efficiency was plotted versus frequency at three relative humidity levels: low (≈25%), mid (≈40%), and high (≈80%). The low level was established by running the blend directly to the reactor without any adjustment. The other humidities were achieved by varying the fraction of the flow which passed through the water-filled Erlenmeyer flask. The percent removal was determined after the humidity had reached a stable value (<3% variation ±), using the procedure described in the previous section. To determine the variability of these plots, three concentration points on the mid humidity curve were chosen and destruction runs for these points were run five times.

Reactor voltage: While the voltage and current waveforms indicate the point at which a plasma is formed in the reactor annulus, they do not indicate whether that plasma is optimized for NO_x destruction. In order to determine an optimum operating point, the removal efficiency was examined for a range of reactor voltages. These tests were conducted at all three humidity levels previously mentioned.

Residence time: The ability of a reactor to process contaminated gases at relatively high rates increases its commercial viability. For this reason, the effect of residence time on destruction efficiency was examined. Previous researchers (Chakrabarti et al. 1995) have established a relationship between destruction efficiency and residence time as a function of number of voltage cycles (frequency). For this reason, destruction efficiency at a set flowrate (residence time) was examined for several frequencies, using techniques described in the destruction efficiency section to determine percent removal. Three points were selected, and repeated runs were performed, to determine the variability (error bars) of the relationship.

Statistical analysis: To establish the repeatability of the process, a statistical analysis was conducted at optimized residence time, concentration, humidity, frequency, and reactor voltage conditions. The removal efficiency was determined as before, except the reactor was turned off and the NO_x flow was interrupted between each run to allow the detector to return to a zero reading. Flow was reestablished and the reactor was turned back on, once a stabilized NO_x concentration was achieved and recorded. This procedure was repeated eight times, and the mean and standard deviation were determined.

Ozone production: The similarity of these DBD reactors to ozonators raises the possibility of high ozone production rates. Since this is of special concern for an automobile emissions application, the amount of ozone produced by the reactor was examined. The measurement was made using an iodometric titration for residual ozone, Standard Method #422 (APHA et al. 1981). In this method, the effluent from the reactor was bubbled through a series of two 500 ml Erlenmeyer flasks filled with 400 ml of a potassium iodide solution. The bubbling continued until the first flask turned a deep

yellow and the second just began to turn yellow. The elapsed time was recorded in order to determine the volume of gas bubbled through the system. Then the flasks were removed and a back titration was performed on the solution in the first flask, using a sodium thiosulfate titrant and starch indicator. The ozone concentration was equal to

$$C_{ozone} = \frac{(T)(N)(24{,}000)}{A} \qquad [16]$$

where: C_{ozone}=ozone concentration of gas (mg/L)
T=volume of sodium thiosulfate titrant (ml)
N=normality of sodium thiosulfate (equivalents/L)
24,000=conversion factor
A=volume of sample bubbled (ml).

Extended operation: In a commercial or industrial setting, these reactors would most likely be operated over extended periods. For this reason, the thermal stability of the system was examined. The temperature of the effluent flow was measured using the digital hygrometer/thermometer mentioned previously. An optimized operating point was selected, and temperature readings were taken periodically for 14 hours. The reactor temperature versus time was then plotted.

Ignition coil as power supply: As previously mentioned, the HEI ignition coil was examined as a possible power supply for the DBD reactor. First, the coil was added to the circuit in Figure 10 in place of the transformer. A Variac was used in place of the signal generator due to previously mentioned limitations of the generator at frequencies less than 100 hertz. The Variac was set to 12 volts rms input to the coil, and destruction efficiency was examined using previously mentioned methods.

RESULTS AND DISCUSSION

> I know not anything more pleasant, or more instructive, than to compare experience with expectation, or to register from time to time the difference between idea and reality. It is by this kind of observation that we grow daily less liable to be disappointed.
>
> Samuel Johnson, Life of Samuel Johnson

General Comments

The process variables were investigated using the procedures described in the previous chapter. In general, these variables were examined to determine the overall applicability of the reactors in a commercial setting.

Power Analysis Results

The power determinations were made using the methods described in the previous chapter. The results presented here primarily examine the relationship between secondary (reactor) voltage and secondary power. Since previous theses have investigated the relationship of apparent primary power and frequency at set primary voltages, a sample graph of this type is presented in Appendix B. In addition, the complete results and data from this section are included in Appendix C.

First, the apparent secondary power (calculated by multiplying secondary voltage and current) was plotted versus the primary voltage. Secondary voltage was actually the voltage across the reactor (measured by the Fluke high-voltage probe, not the other high-voltage probe which was only reliable at 60 hertz). Figures 13 and 14 plot this data for Reactors A and B, respectively.

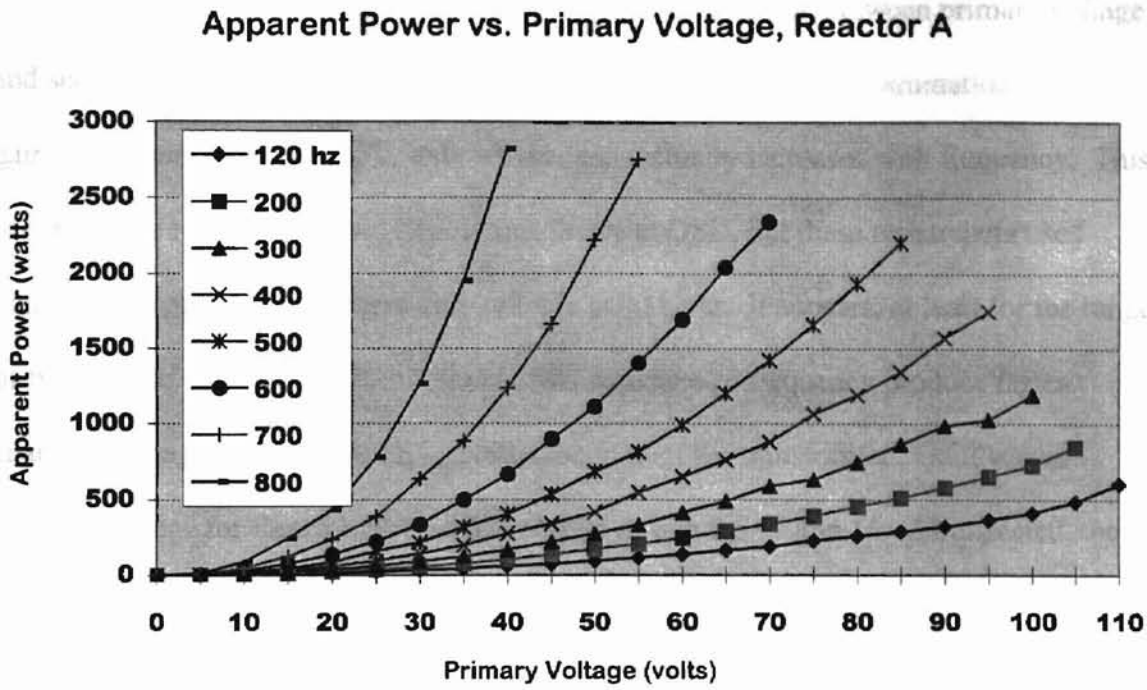

Figure 13: Apparent power plot versus primary voltage

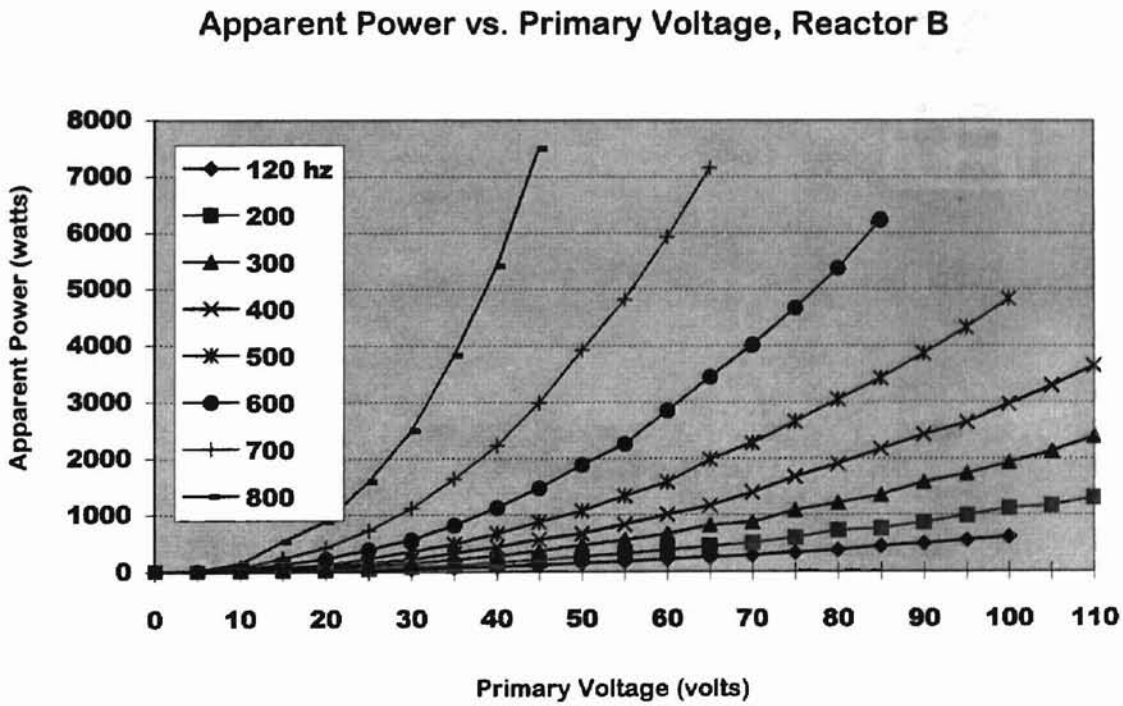

Figure 14: Apparent power plot versus primary voltage

These plots seem to indicate an exponential relationship between primary voltage and secondary power, especially at higher frequencies. However, examination of the gain of the transformer (V_{out}/V_{in}) shows that gain actually increases with frequency. This is contrary to results presented in previous theses at OSU, but these researchers used high-voltage probes which were only reliable at 60 hertz. It appears, at least for the range of frequencies examined in this research, that increases in frequency produce faster changes in magnetic flux, which increases the gain of the transformer. Gain versus primary voltage for Reactors A and B is plotted in Figures 15 and 16. As expected, the data for both reactors shows similar trends.

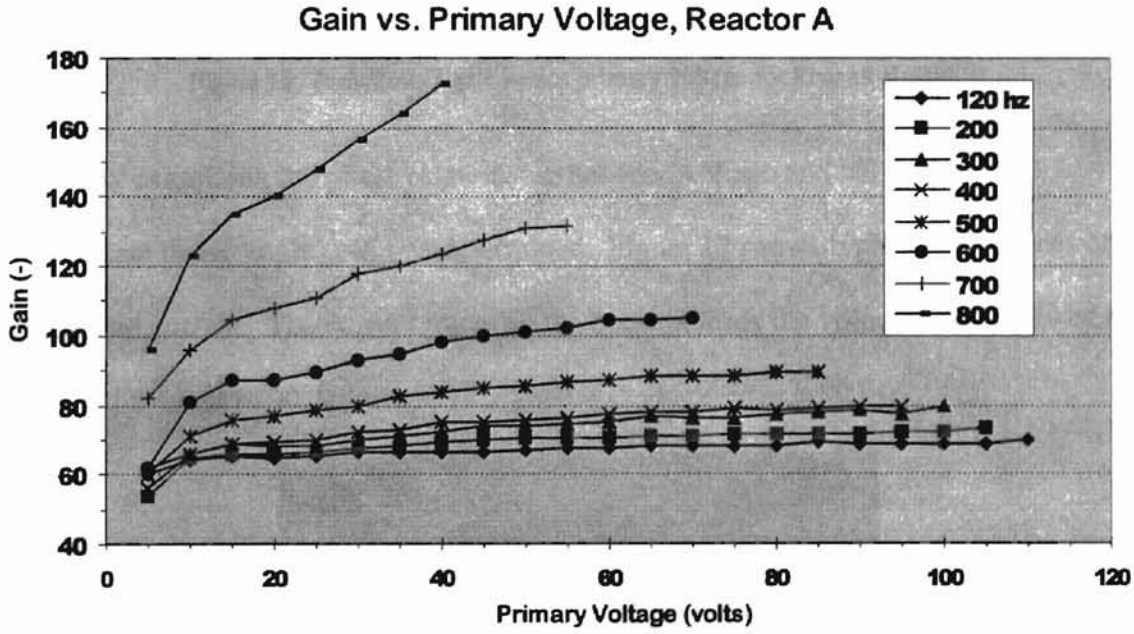

Figure 15: Transformer gain versus primary voltage for Reactor A data

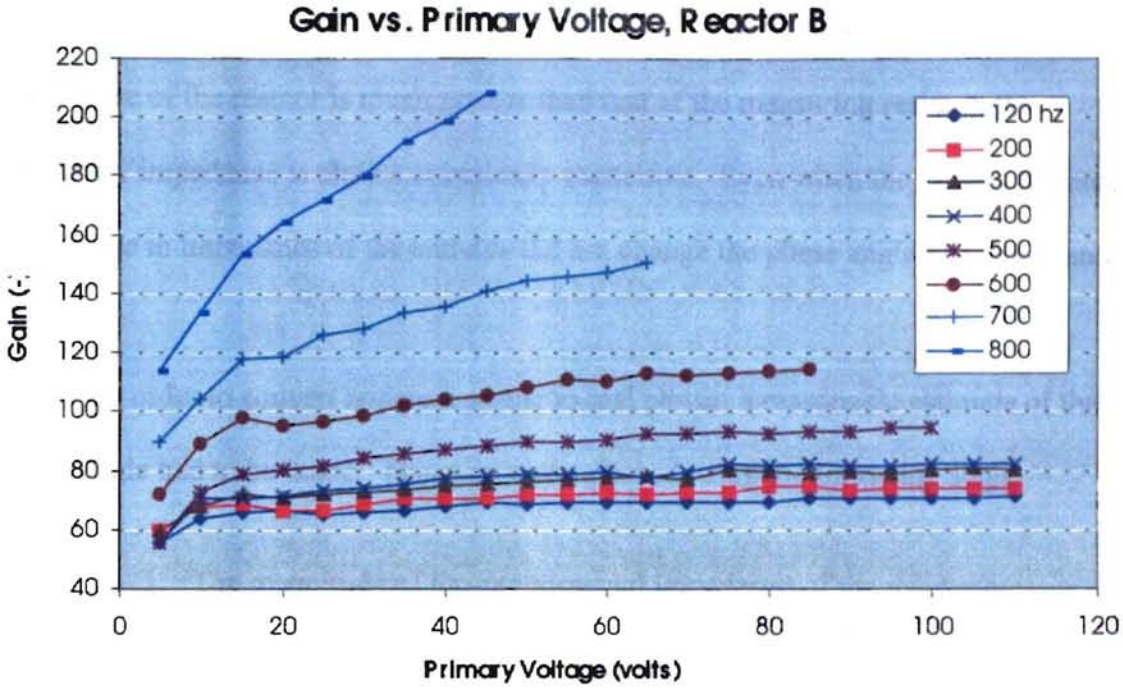

Figure 16: Transformer gain versus primary voltage for Reactor B data

By examining the phase relationship between voltage and current, the approximate phase angle could be determined. Figure 17 shows typical CRO traces of voltage and current. The current trace, on the bottom, leads the voltage trace by ¼ of a period, equivalent to 90 degrees.

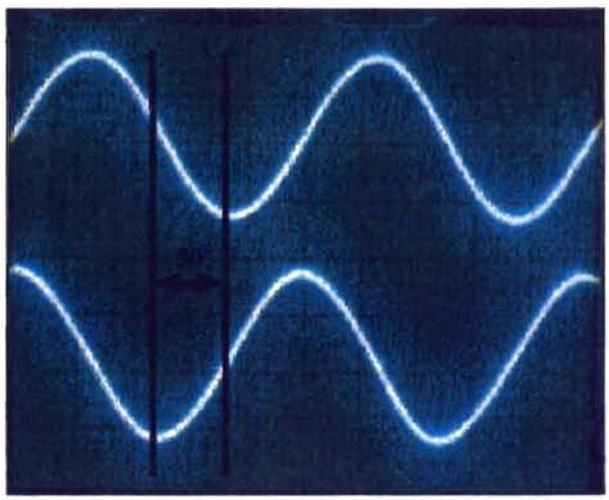

Figure 17: Typical voltage and current phase relationship

This ≈90° relationship was constant for all secondary voltages. Since the impedance of the reactor is much greater than that of the measuring resistor, the secondary impedance is almost completely capacitive. Even when the plasma formed, the change in impedance of the annulus did not change the phase angle of voltage and current.

In order to convert apparent power to real power, a reasonable estimate of the phase angle had to be made. This was accomplished using the following steps:

1. The magnitude of the experimental impedance of the reactor/measuring resistor combination was calculated by dividing the voltage by the current for each primary voltage setting. This was found to be nearly constant over all voltages at a set frequency, with a maximum percent deviation of 5.8%.

2. The theoretical impedance, phase angle, and power factor were calculated using equations [11] and [12] and known values of resistance, capacitance, and frequency. The theoretical phase angle ranged from 89.4° at 120 hertz to 86.3° at 800 hertz, due to decreasing capacitive impedance.

3. The two values were compared to establish the validity of using the theoretical phase angle to calculate the experimental real power.

Tables 6 and 7 present the comparison for Reactors A and B at various frequencies. While the ratio is not equal to 1.0 due to stray impedance in the circuit, the fairly low standard deviations indicate the phase angle and power factor do not vary as the plasma forms in the reactor.

Frequency	120 Hz	200 Hz	300 Hz	400 Hz	500 Hz	600 Hz	700 Hz	800 Hz
Z_{theory}/Z_{exp}	0.89	0.85	0.82	0.93	0.92	0.90	0.89	0.90
Standard Dev.	0.056	0.018	0.034	0.043	0.037	0.027	0.012	0.015

Table 6: Impedance ratios and standard deviations for Reactor A

Frequency	120 Hz	200 Hz	300 Hz	400 Hz	500 Hz	600 Hz	700 Hz	800 Hz
Z_{theory}/Z_{exp}	0.94	0.88	0.92	1.00	0.96	0.95	0.94	0.96
Standard Dev.	0.051	0.023	0.046	0.049	0.027	0.021	0.013	0.063

Table 7: Impedance ratios and standard deviations for Reactor B

These calculations lend credence to the use of the theoretical phase angle and power factor to calculate real secondary power. Applying these values, Figures 18 and 19 plot real secondary power versus secondary voltage for Reactors A and B.

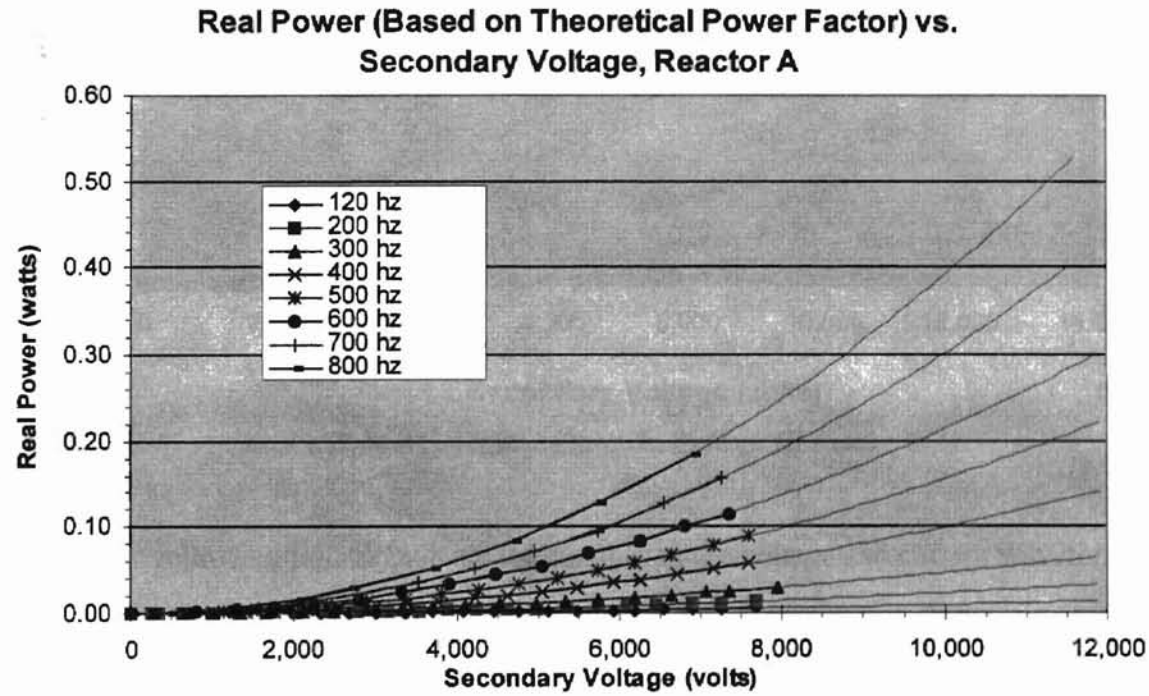

Figure 18: Real power versus secondary voltage for Reactor A

As the secondary voltage approached what was needed for plasma formation, the current waveform became irregular (refer to Figure 22) and unreliable to use for calculation of power consumption. This made it necessary to extrapolate the power curves to higher secondary voltages. The trendlines were all second-order polynomial curve fits with correlation coefficients ≥0.99. While the changing shape of the current

waveform may indicate a change in power curve trends, examination of the voltage/current phase relationship and the "averaged" current amplitude indicated the extrapolation was valid.

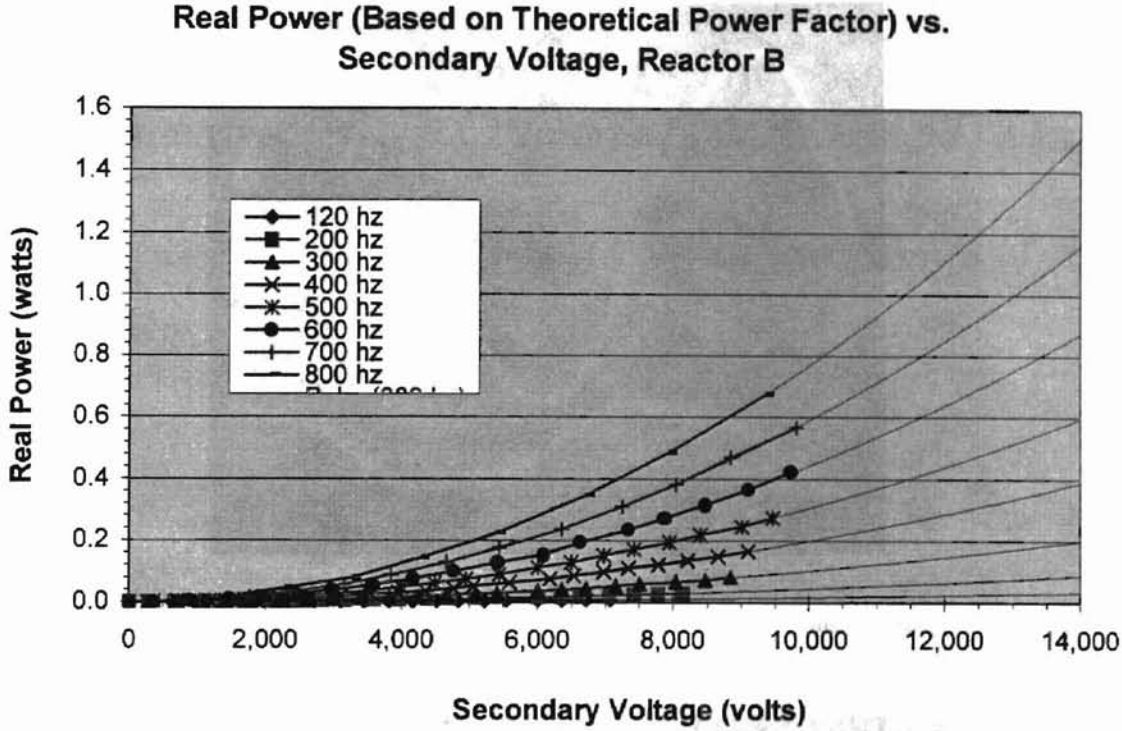

Figure 19: Real power versus secondary voltage for Reactor B

The following figures indicate the changes in the voltage and current waveforms as the plasma formed in the annulus. As previously mentioned, the phase relationship between voltage and current stayed the same, but minor variations in the voltage shape and more pronounced changes in the current waveform occurred as the plasma formed. Figure 20 is a photograph of both traces. Figure 21 indicates only slight alterations in the voltage form, especially on the leading edge of peaks. Figure 22 exhibits the changes in secondary current which accompany plasma formation. These determinations were verified by repeating with a liquid electrode plasma (Graham 1997) and comparing the point at which a visible plasma appeared and the associated changes in voltage and

current waveforms. This reactor exhibited the same trends in system and secondary power consumption despite a differing geometry and dissimilar materials of construction. Data and graphs from these measurements are included in Appendix C.

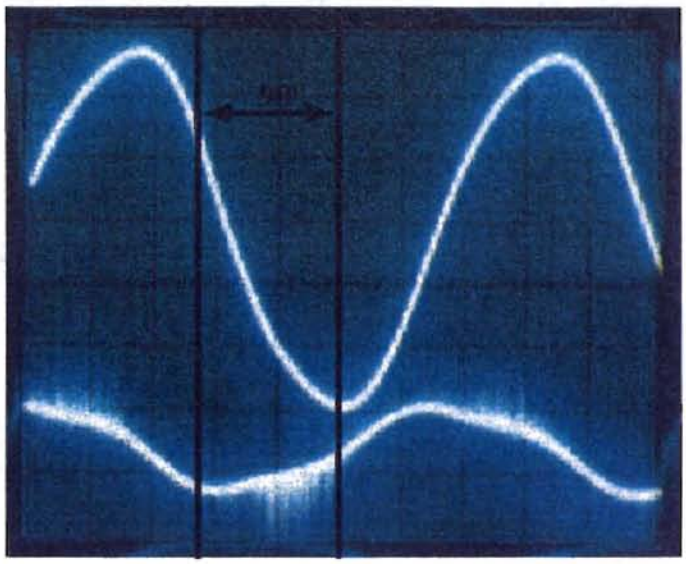

Figure 20: Voltage and current CRO traces at plasma-forming voltages

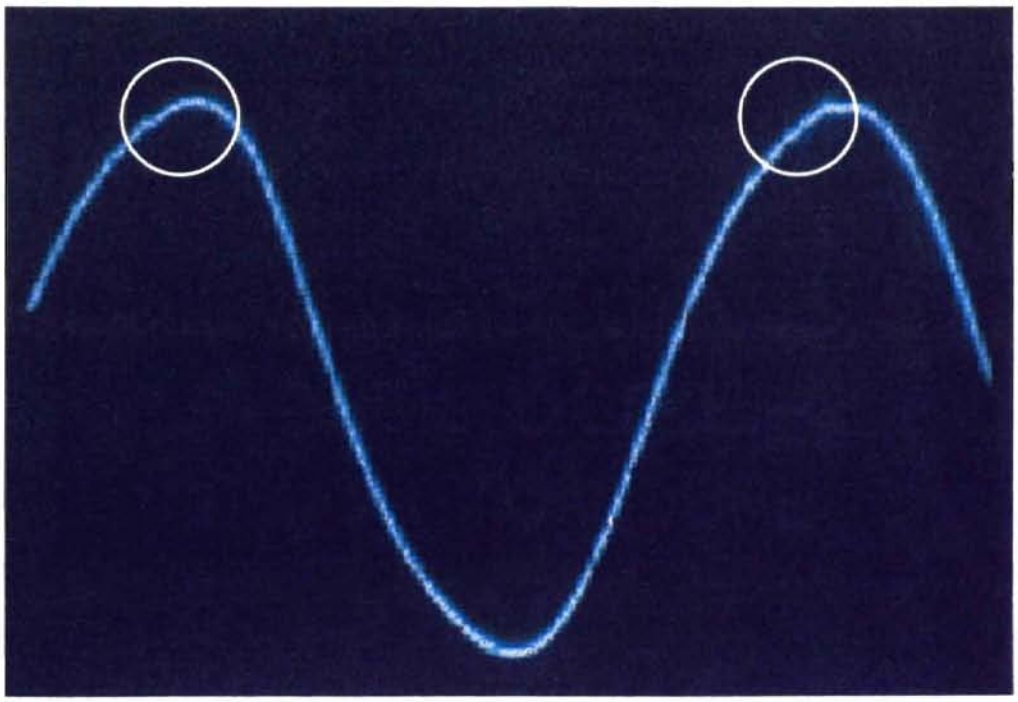

Figure 21: Voltage trace at plasma-forming voltages (note slight breaks near peaks)

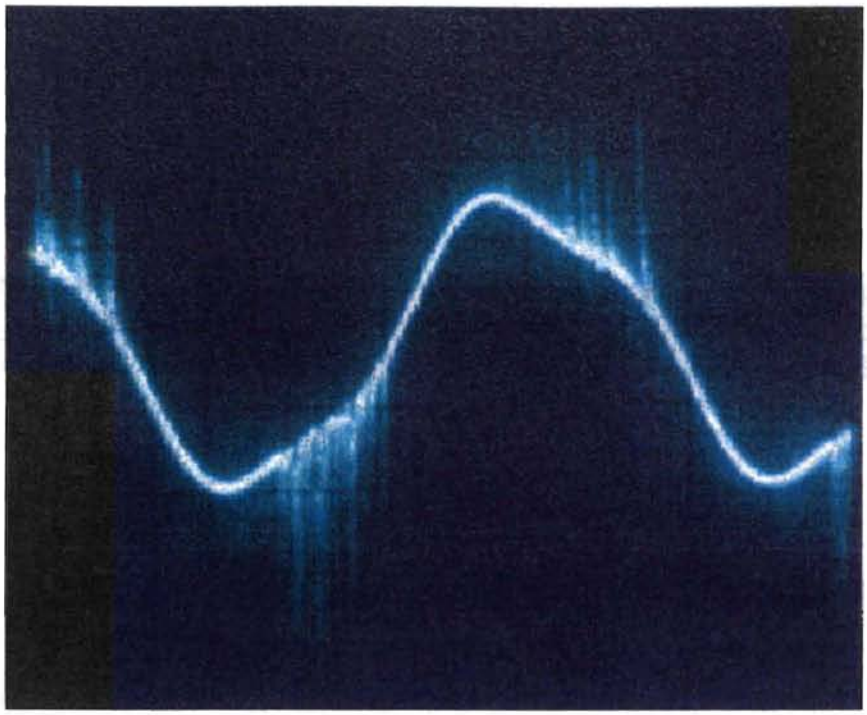

Figure 22: Current trace at plasma-forming voltages (note discharge spikes)

The fuzziness of the current waveform began at approximately 6,000 volts, as the gas in the annulus began to ionize. However, destruction experiments (see reactor voltage analysis section) confirmed that the voltage waveform changes, namely the "breaks" near the peaks, were the best indication of plasma formation. The estimated critical voltage of plasma formation for each reactor is discussed in the following section.

In order to determine the ratio of real power used by the reactor to total real power used by the entire system (frequency generator, transformer, and reactor), a wattmeter was used to measure real power consumed by the entire circuit. A comparison of total power and power used just by the reactor at three operating points is presented in Table 8. Obviously, the power used by the reactor is a tiny fraction of that used to power the whole system. While the power supplied to the reactor *increases* with frequency, the

power used by the circuit *decreases*. Obviously, the system which supplies power to the reactor is not optimized. As mentioned in the Procedure chapter, once a desired operating point is selected, a power supply circuit should be designed which allows maximum power transfer to the reactor itself.

Frequency (hertz)	Reactor Power (watts)	Total System Power (watts)	Fraction of Power Used by Reactor (-)
200	0.022	>150	<0.000147
300	0.043	144	0.000299
400	0.010	108	0.000926

Table 8: Reactor power and total power comparison

Gap Width Comparison Results

Examination of Figures 18 and 19 indicates Reactor B's power consumption was greater than that of Reactor A's. Since Reactor B has a slightly higher measured capacitance than A (refer to Table 4), its impedance is lower, resulting in higher power consumption. This most likely accounts for the majority of the difference between Figures 18 and 19.

The increased gap width *did* account for a significant difference between the two reactors in the category of plasma-formation voltage. These approximate critical voltages are outlined in Table 9.

	Gap Width	Critical Voltage
Reactor A	0.67 cm	9,500 volts
Reactor B	1.38 cm	over 14,000 volts

Table 9: Plasma-formation voltages

Since the transformer used in this experiment was rated at 15,000 volts maximum, any research requiring compound destruction could not be accomplished with Reactor B. While the increased gap width would allow Reactor B to process higher flowrates than Reactor A at the same residence time, the significant increase in power consumption of the reactor at voltages necessary for plasma formation (see Figure 19) indicates its operating costs would be much higher.

Reactors used by other researchers (Chang et al. 1993) with gap widths similar to Reactor B required voltages in the range of 23,000 to 25,000 volts. In future research, it would be desirable to obtain a higher rated transformer to compare removal rates and costs for reactors with higher gap widths.

Reynolds Number Results

Since Reactor A was the only reactor used for destruction experiments, the Reynolds numbers for three residence times were calculated for it only. The results are presented in Table 10 and complete calculations are included in Appendix D.

Residence Time (sec)	Flowrate (m^3/sec)	Reynolds # (-)
5.0	$1.26 * 10^{-5}$	82.6
2.5	$2.51 * 10^{-5}$	165
1.0	$6.28 * 10^{-5}$	413

Table 10: Reynolds numbers for Reactor A flowrates

These numbers are all <2,000 and indicate primarily laminar flow. This indicates a non-uniform velocity profile. Since plasmas are considered a fourth state of matter, it is difficult to have any real notion of the flow regime once the plasma forms.

Destruction Efficiency Results

As previously mentioned, all destruction runs were conducted with Reactor A to insure plasma formation. The tests were conducted using procedures outlined in the preceding chapter. Each variable was examined in turn and the most efficient operating conditions were selected for the subsequent section. The complete data from the destruction efficiency runs is included in Appendix E.

Humidity variation analysis: Initial destruction efficiency investigations were conducted to determine the effect of humidity and influent concentration on removal efficiency. All these runs were conducted at a secondary voltage of 10,500 volts, residence time of 5 seconds, and at a frequency of 400 hertz. Figure 23 illustrates the effect of these two variables on removal efficiency.

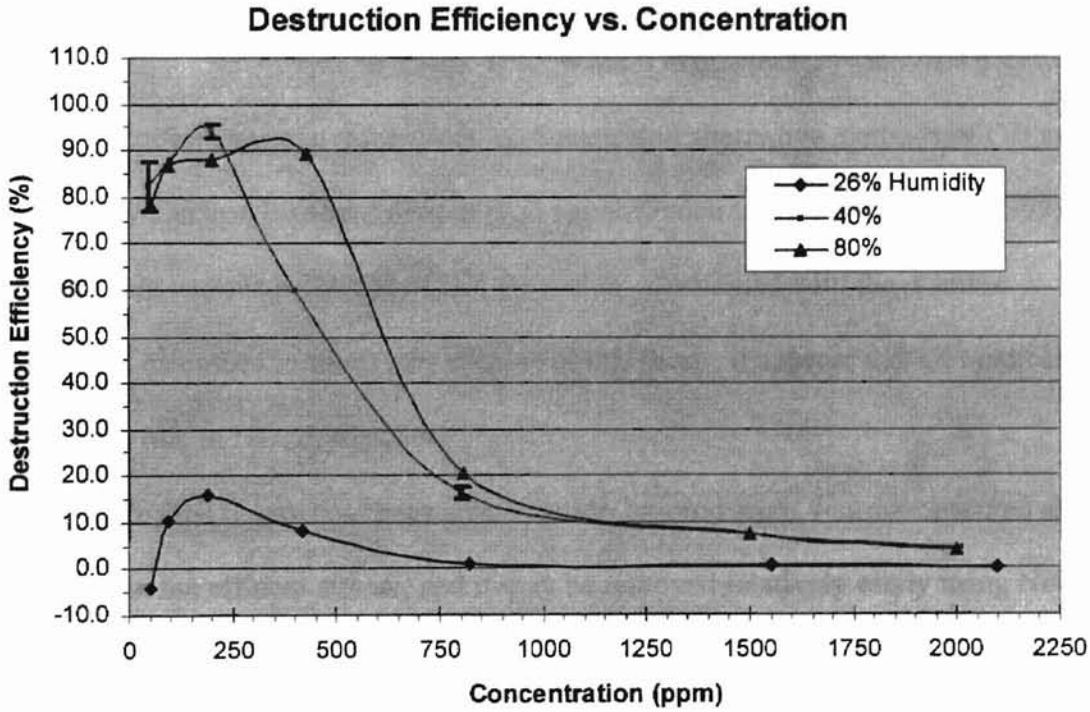

Figure 23: Effects of concentration and humidity on removal efficiency
(error bars on mid humidity curve indicate ± 3 standard deviations)

From the shape of the curves, it becomes apparent that humidity and concentration have extremely pronounced effects upon destruction efficiency. The general shapes of all three humidity curves are similar, but low humidities (directly from compressed cylinders) greatly reduce removal efficiencies. The mid and high humidity curves are essentially identical, but the higher humidity appears to expand the optimum destruction window to higher influent concentrations. The ramifications of these results on the application of the system to auto exhaust will be discussed in the following chapter.

The exact role of humidity (i.e. free H_2O molecules) in NO_x destruction is not known, but previous researchers (Chang et al. 1993) have suggested the following reaction mechanisms:

$$O_3 + h\nu \text{ (photon)} \rightarrow O'(D)^* + O_2$$
$$O_2 + H_2O_{(g)} \rightarrow 2OH$$
$$OH + NO_2 \rightarrow HNO_3$$

*Note: O'(D) indicates oxygen (radical) with raised d-shell electron

In addition, various researchers have presented alternative methods of OH radical formation by electron bombardment of H_2O vapor (Penetrante and Schultheis 1993). These indicate various pathways of OH formation. Combined with the reaction mechanisms discussed in the theory chapter of this thesis, it appears that OH radicals play a significant role in NO_x destruction.

While HNO_3 may not be an ideal reaction by-product, it was not observed as a condensate in the effluent stream, and it may be removed relatively easily using NH_3 neutralization and a variety of aerosol particle removal devices (Chang et al. 1993). In other words, even if HNO_3 production is a side effect of the DBD plasma treatment of

NO_x, the overall effect remains positive. Further studies should try to "trap out" the moisture in the effluent and determine its HNO_3 concentration.

Reactor voltage analysis: In an attempt to minimize the power consumption of the reactor, the minimum voltage resulting in NO_x destruction was sought. In this portion of the destruction experiments, the following conditions were constant:

- Frequency: 400 hertz
- Residence time: 5 seconds
- Influent concentration: 200 ppm

Figure 24 displays the relationship of reactor voltage and destruction efficiency.

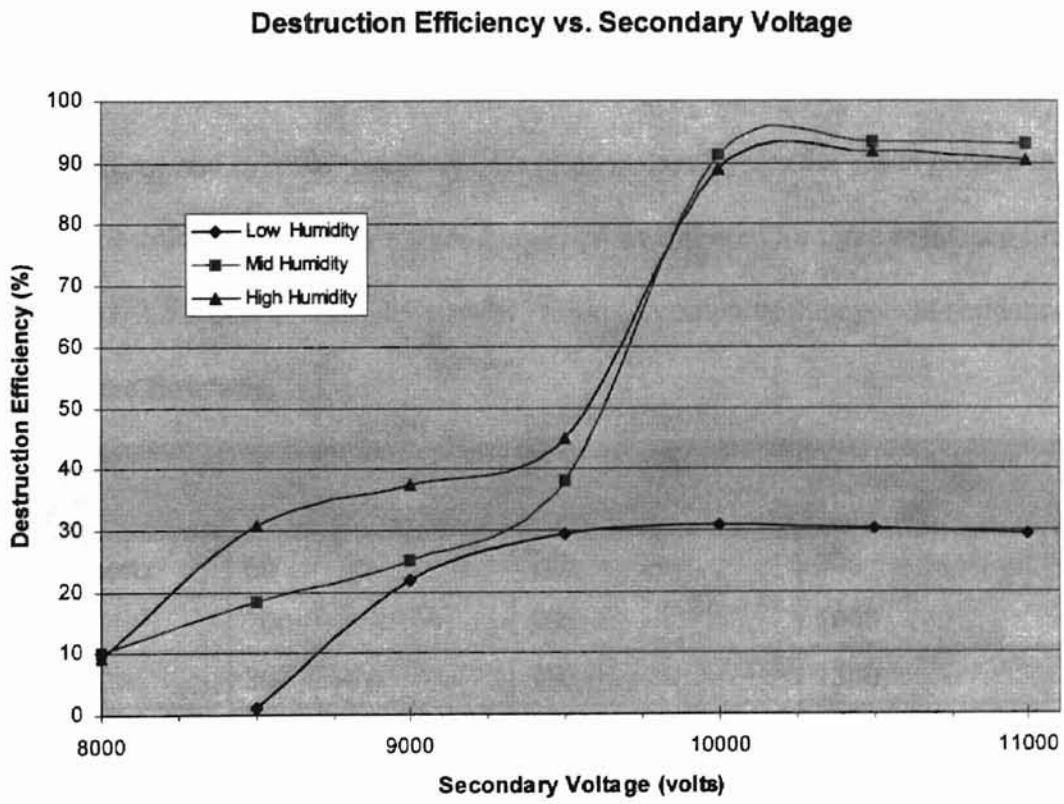

Figure 24: Destruction efficiency versus reactor voltage plot

A sharp increase in destruction efficiency (for mid and high humidity curves) accompanied the increase of reactor voltage from 9,000 to 10,000 volts. This corresponded to the formation of a plasma in the annulus. The removal percentages peaked at 10,000 volts and remained relatively constant up to 11,000 volts.

As seen previously, mid and high level humidities greatly increased destruction efficiencies. The mid and high humidity curves were essentially identical, except for slightly higher destruction levels at low voltages for the high humidity curve. This may be due to water vapor aiding in plasma formation at high humidity levels.

To provide for maximum destruction at the lowest operating costs while insuring the presence of a plasma in the annulus, 10,000 volts was selected as the operating voltage for the remainder of the investigations.

Residence time and frequency analysis: To better understand the relationship between residence time and cyclical residence time (# of voltage cycles the gas is present in the reactor), destruction efficiency versus frequency was plotted for three residence times, 1.0 second, 2.5 seconds, and 5.0 seconds. Table 11 compares the cyclical residence times for the three flowrates.

Frequency	Cyclical residence time (θ = 1.0 sec)	Cyclical residence time (θ = 2.5 sec)	Cyclical residence time (θ = 5.0 sec)
60 hertz	60	150	300
200	200	500	1000
300	300	750	1500
400	400	1000	2000
500	500	1250	2500
600	600	1500	3000

Table 11: Comparison of cyclical and traditional residence times

The observed destruction efficiencies are plotted in Figure 25 and Figure 26. Figure 25 observes the relationship of destruction efficiency versus frequency for three residence times, while Figure 26 plots destruction efficiency versus cyclical residence time (utilizing all three residence times). The error bars in Figure 26 indicate decreasing variability with higher cyclical residence times. These bars are relatively large, since the 500, 1000, and 1500 cycle times each had data from two traditional residence times (either 2.5 and 5.0 seconds or 1.0 and 2.5 seconds).

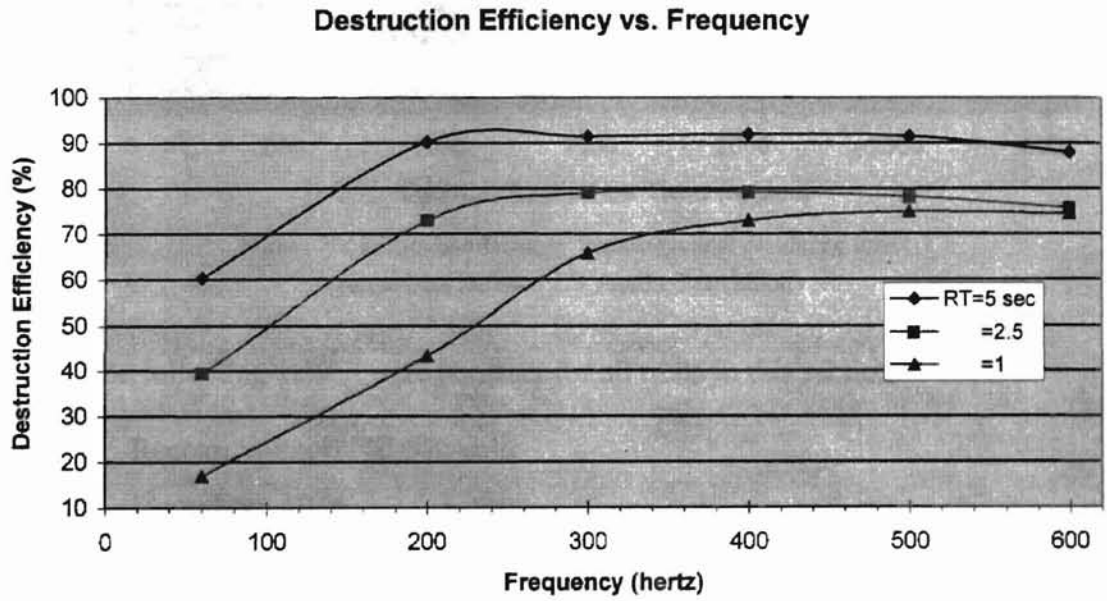

Figure 25: Removal efficiencies versus frequency for three flowrates

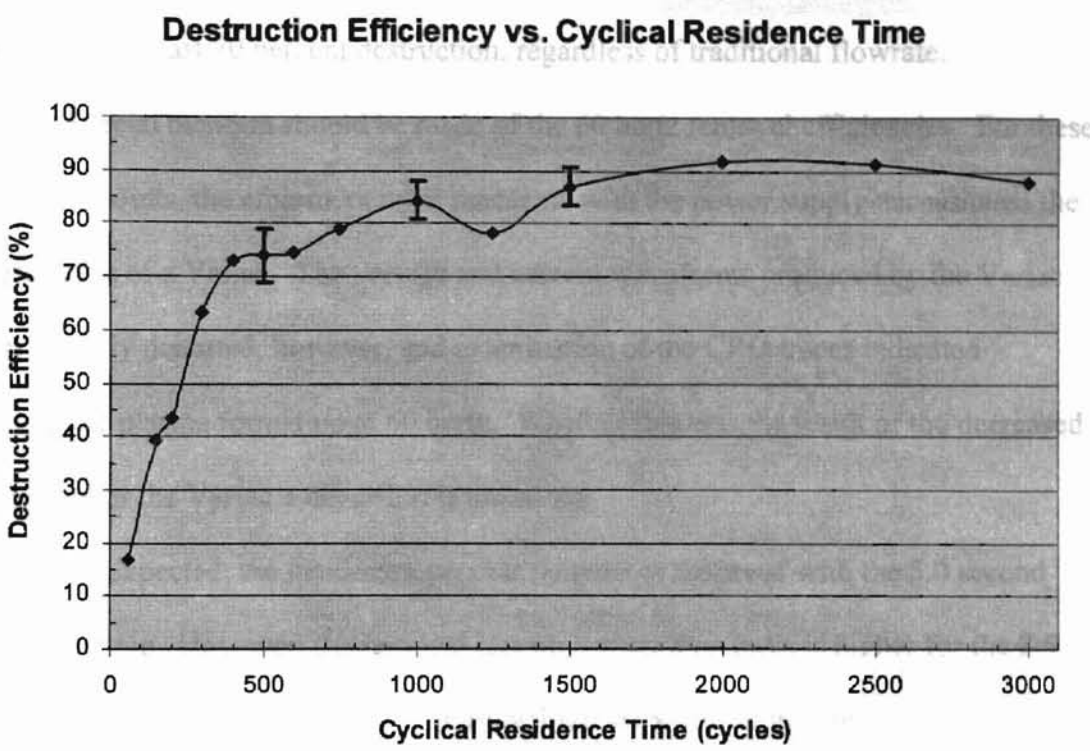

Figure 26: Removal efficiency versus cyclical residence time
(error bars indicate ± 1 standard deviation)

The following values were constant for all trials in this section:

- Reactor voltage: 10,000 volts
- Humidity: 40 %
- Influent concentration: 200 ppm

Examination of the three flowrate curves indicates a maximum removal rate is achieved for each. Increased cyclical residence time that accompanies higher frequencies appears to increase removal rates, especially for the 1.0 second residence time. Unfortunately, higher frequencies result in higher power use by the reactor. All three curves seem to approach an asymptotic maximum removal, possibly indicating reaction kinetics prevent any further destruction at each humidity level, regardless of residence

time. Figure 26 indicates that increasing the cyclical residence time over 400 cycles guarantees at least 70 percent destruction, regardless of traditional flowrate.

Special mention should be made of the 60 hertz removal efficiencies. For these operating points, the aforementioned problems with the power supply necessitated the substitution of a Variac. The voltage and current waveforms produced by the Variac were slightly distorted, however, and examination of the CRO traces indicated incomplete plasma formation at 60 hertz. Whether this was the result of the decreased frequency or the Variac's distortion is unknown.

As expected, the maximum percent removal is achieved with the 5.0 second residence time. However, the removal rate on a *mass/time* basis is higher for the 2.5 and 1.0 second flowrates. The preferred removal rate depends on the application of the reactor. A more thorough comparison of removal rates and operating costs is presented in a subsequent section.

Statistical analysis: To get an idea of the reproducibility of the experimental results, a statistical analysis of a typical operation point was conducted. The following variables were constant for all trials:

- Reactor voltage: 10,000 volts
- Humidity: 40%
- Influent concentration: 200 ppm
- Frequency: 300 hertz
- Residence time: 1.0 second

The methods used to insure the statistical independence of each trial were outlined in the previous chapter. The results from this section are summarized in Table 12.

Trial Number	Removal Efficiency
1	51.3
2	51.5
3	51.2
4	49.1
5	51.0
6	51.2
7	52.2
8	52.0
Average Removal Efficiency	51.2
Standard Deviation	0.953

Table 12: Reproducibility statistical analysis

The standard deviation is less than 1%, an indication that destruction efficiency results are reproducible with significant uniformity. It should be noted that all the destruction efficiencies observed in this section are lower than those observed for the corresponding operating point in the previous section. The reactor was disassembled and examined after these trials. The neoprene stoppers were found to be splitting and brittle. This produced current leakage in the trials and most likely accounted for the decreased removal efficiencies. Further discussion of the stopper degradation is presented in the extended operation section.

Summary of operating costs and removal rates: At this point, it is useful to compare operating costs and removal rates to get an idea of possible operating conditions for the system. The operating costs listed in Table 13 are based upon a typical electricity rate of $0.11/kWh, power consumption from Figure 18 (power consumption*electricity rate/hour*24 hours/day = operating costs), and destruction percentages from Figure 25. Again, the power consumption used is that of the reactor only, not the entire system.

This assumes an optimized power supply will be able to supply power to the reactor with only small losses elsewhere.

Frequency (hertz)	Operating Costs ($/day)	Destruction % (θ=5.0 sec)	Destruction % (θ=2.5 sec)	Destruction % (θ=1.0 sec)
200	$0.00006	90	73	43
300	$0.00012	92	79	66
400	$0.00026	92	79	73

Table 13: Operating costs and removal efficiencies for three frequencies

By substituting in the corresponding flowrates for each residence time and multiplying by the operating costs, the grams of NO_x removed per day and cost per gram of NO_x removed may be determined. These results are presented in Table 14.

Frequency (hertz)	g NOx destroyed/day *$/NOx destroyed* (θ=5.0 sec)	g NOx destroyed/day *$/NOx destroyed* (θ=2.5 sec)	g NOx destroyed/day *$/NOx destroyed* (θ=1.0 sec)
200	0.254 *$0.00024*	0.413 *$0.00015*	0.607 *$0.00010*
300	0.260 *$0.00047*	0.447 *$0.00027*	0.932 *$0.00013*
400	0.260 *$0.00099*	0.447 *$0.00058*	1.030 *$0.00025*

Table 14: Removal rates and costs for three frequencies

Yet again, the ideal operating point depends upon the treatment objectives. On a cost/gram basis, the optimum operating point is at 200 hertz and 1.0 second residence time. If maximum destruction is the objective, increasing the frequency to 300 hertz significantly improves grams of NO_x destroyed per day. If maximum percent removal is desired, a higher residence time, 2.5 or 5.0 seconds, will improve destruction percentages. Operating and regulatory requirements would likely dictate which operating point is selected.

Ozone Production

Since ozone is a common by-product of these reactors, its production rates and concentrations are of some concern. A number of iodometric titrations were performed to determine ozone concentrations and production. These are summarized in Table 15 and complete titration data is included in Appendix F. The following conditions were constant for all ozone production trials:

- Reactor voltage: 10,000 volts
- Influent NO_x concentration: 200 ppm
- Humidity: 40%

Frequency (hertz)	Residence Time (sec)	Average Ozone Concentration (mg/L)	Average Ozone Production (mg O_3/mg NO_x removed)
300	1.0	0.55	3.22
300	5.0	0.59	2.47
400	1.0	0.55	2.88

Table 15: Ozone production results

From this data, it appears ozone concentration is independent of the frequency of applied voltage, but does decrease with increased residence times. This indicates the reactions which produce ozone occur relatively quickly and do not continue (or continue at a significantly lower rate) with increased residence times. These results generally agree with those of previous researchers (Graham 1997). If removal rates (from the residence time analysis section) are considered as well, the lowest ozone production per NO_x removal occurs at higher residence times, due largely to increased removal efficiencies. In other words, since ozone concentration only increases slightly with longer residence times, and removal efficiency increases more markedly with longer residence times; the net production rate per removal rate is lower.

While the ozone production is a matter of some concern, the removal of ozone is generally accomplished much more easily than that of NO_x, especially at the relatively low levels observed in this research.

Extended Operation

The thermal stability of the unit when operated for extended periods is a concern as well. For this reason, the reactor was operated for 14 hours and the effluent gas temperature was recorded to determine any heating trends. For this trial, the unit was operated under the following conditions:

- Frequency: 300 hertz
- Humidity: 40%
- Residence time: 2.5 seconds
- Influent concentration: 200 ppm
- Reactor voltage: 10,000 volts

Figure 27 plots the effluent gas temperature versus time.

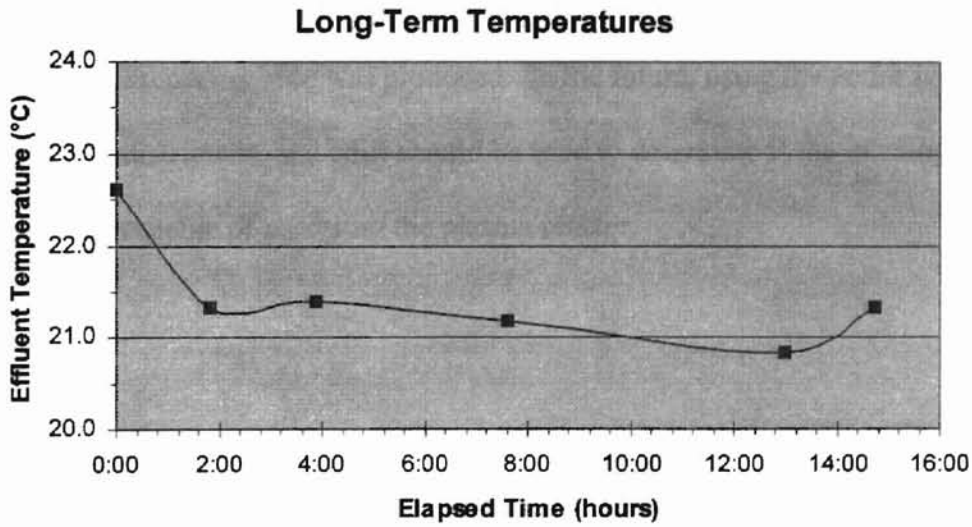

Figure 27: Effluent temperature versus time

This plot indicates no real trends in reactor effluent temperature. The fluctuations which occur appear to be the result of variability in the lab's HVAC system, since hours 4 to 13 corresponded to nighttime, or the coldest outdoor temperatures. This data indicates the reactor experiences no quantifiable temperature increase, even when operating for as long as fourteen hours.

One significant effect of extended operation, noted previously in the statistical analysis section, was the observed degradation of the neoprene stoppers. Inspection of the stoppers before and after the trial suggests long-term exposure to the plasma environment (high electrical fields and ozone) causes notable corruption of the material. Further suggestions for remedying this situation are presented in the summary.

Ignition Coil as a Power Supply

As previously mentioned, the possibility of employing an automobile ignition coil in place of the transformer was examined. Unfortunately, the extremely low impedance (calculated to be ≈2.6 ohms) of the coil prevented applying a great enough voltage without exceeding the amperage rating of the Variac. A maximum of only 3,000 volts across the coil's secondary side was produced. In the future, using the entire ignition system (battery, distributor, and coil) should be tried to determine if the existing components are capable of powering the plasma reactor.

ENGINEERING APPLICATIONS

> To define it rudely but not inaptly, engineering . . . is the art of doing that well with one dollar, which any bungler can do with two after a fashion.
>
> Arthur Mellen Wellington,
> The Economic Theory of the Location of Railways

One of the primary goals of this research was to determine the applicability of a DBD plasma reactor to the treatment of automobile exhaust. This involves consideration of a number of factors, including treatment rates, power requirements, removal efficiencies, regulatory (EPA) requirements, and competing technologies.

The results of this research certainly indicate DBD plasma reactors can successfully remove large fractions of NO_x in concentrations up to 750 ppm. Since most sources list NO_x production in terms of grams/mile, it is difficult to determine if this is an adequate range of treatable influent concentrations. The Society of Automotive Engineers recommends calibration of NO_x detectors (which measure auto exhaust concentrations) up to 250 ppm for cars manufactured since 1976 (SAE 1995). This likely provides for measurement of exhausts which pass over fouled catalytic converters, or with concentrations equal to those directly downstream of the engine. Older sources indicate NO_x production in the range of 450 to 750 ppm (Patterson and Henein 1972). This combination of sources suggests DBD technology can treat typical exhaust levels.

The need to meet EPA requirements for NO_x effluent levels (currently 0.4 grams/mile), requires percent removals in the range of those produced by existing catalytic converters. Estimates for current systems range from 70% to 90% removal efficiency (Schäfer and van Basshuysen 1995). These removal efficiencies were routinely observed for the 5.0 second residence time and nearly 80% removal occurred

for the 2.5 second residence time (refer to Figure 25). This indicates removal efficiencies comparable to those of existing methods.

Further tests need to be conducted to determine typical flowrates and residence times in automobile exhaust systems. In addition, measurements of the typical humidity and temperature of automobile exhaust should be taken to determine if existing materials are suitable.

The DBD reactor presents a number of practical advantages over traditional catalytic conversion. First, the reactor consists of an open tube, which does not produce the back-pressure found in converters. This back-pressure reduces the fuel economy of automobiles. Second, the proposed system, using Teflon lining, is extremely unlikely to become fouled by soot and other particles in automobile exhaust. Again, this presents a practical advantage to existing systems. Finally, the materials that make up the reactor and the potential voltage source (already present in all cars) are much less expensive than the metals and ceramics of normal catalytic converters. While the system used in this research is similar to the one used in the previously mentioned patented systems (Rich 1994, Rich 1995), there appear to be enough signficant differences in the system to prevent any possibility of infringement.

The advances in catalytic converter technology discussed in the Introduction promise improved overall removal rates and performance for contaminants. Unfortunately, these advances do not generally improve the rate of NO_x removal. If the proposed system provides similar removal of hydrocarbons and carbon monoxide, it may prove to be a very attractive alternative to complex second-generation catalytic converters.

CONCLUSIONS AND RECOMMENDATIONS

> For undemocratic reasons and for motives not of State,
> They arrive at their conclusions— largely inarticulate.
> Being void of self-expression they confide their views to none;
> But sometimes in a smoking room, one learns why things were done.
>
> Rudyard Kipling (speaking of scientists), The Puzzler

This study of DBD plasma destruction of NO_x compounds reached a number of conclusions concerning the removal efficiency, power consumption, and general performance of the system.

- Power consumption increases with increased voltage and increased frequency.
- By using a CRO and examining the secondary current/secondary voltage phase relationship, estimates of power factor and real power may be made.
- The phase angle of the secondary current to secondary voltage stays at essentially 90° (power factor near zero), even when a plasma forms in the reactor annulus. This indicates the impedance remains predominantly capacitive throughout.
- The tuning of the system observed by other OSU researchers did not occur in this study. It is believed the curves generated by previous research were erroneous due to the use of high-voltage probes not designed to operate at frequencies other than 60 hertz.
- The most reliable (non-visual) evidence of plasma formation is breaks in the voltage CRO trace. This is accompanied by significant discharge spikes in the current trace.
- Increasing reactor gap width does not automatically increase power consumption, if the overall impedance remains unchanged. However, increasing gap width requires increased reactor voltages to produce a plasma.

- The presence of relatively moderate humidity levels increases destruction efficiency greatly, from a maximum of 15% at 27% humidity to a maximum of over 90% removal at 40% humidity.
- Maximum destruction efficiency occurs for concentrations less than 750 ppm.
- Increasing cyclical residence time (frequency) improves destruction efficiency slightly for short residence times (under 5.0 seconds). Increasing the cyclical residence time to >400 cycles guarantees at least 70 percent destruction, regardless of flowrate.
- While maximum destruction efficiency (on a percentage basis) occurs at high residence times, maximum removal rates (mass/time) occur at lower residence times.
- Destruction efficiency appears to be relatively constant, if all operating conditions remain unchanged.
- Ozone production does occur, with only slightly higher concentrations accompanying longer residence times.
- No significant effluent temperature increases result from long-term operation.
- Operating costs range from $0.00006 to $0.00026 per day, depending upon applied frequency. This is based on power use of the reactor only.

To increase the confidence in the reactor's commercial applicability and to better evaluate the effects of parameters such as gap width, a number of procedural and material modifications should be made.

- A more reliable power source, capable of operating over a wider range of frequencies and which doesn't create feedback loops with the transformers, should be obtained.

- A CRO with a multiplying function, which would allow better estimation of real power consumption, should be obtained as well.

- To better evaluate the unit in an automobile exhaust application, an actual ignition system should be used as the power supply and a configuration similar to a typical tailpipe should be examined. The first step in this process should include rough determinations of the humidity, temperature, and flowrates of car exhaust. Then, a bench-scale system could be designed and applied to an actual exhaust stream and evaluated for NO_x removal, hydrocarbon destruction, and other properties.

Considering the overall success of the destruction runs and relatively low power consumption and operating costs observed, it appears that the unit may have multiple applications in the area of NO_x removal.

REFERENCES

APHA, AWWA, and WPCF. Method 422 "Ozone (Residual)," Standard Methods for the Examination of Water and Wastewater. 15th edition, 1981.

Atkins, P.W. and Beran, J.A. General Chemistry. 2nd edition, 1990.

Baddour, R.F. and Timmins, R.S. The Application of Plasmas to Chemical Processing. Massachusetts Institute of Technology, 1967.

Boenig, H.V. Plasma Science and Technology. Cornell University Press, 1982.

Chaikin, D. "How it Works: Catalytic Converter," Popular Mechanics. April 1992.

Chakrabarti A., Mizuno, A., Shimizu, K. Matsuoka, T., Furuta, S. "Gas Cleaning with Semi-Wet Type Plasma Reactor," IEEE Transaction on Industry Applications. Vol. 31, No. 3, May/June 1995.

Chang, M.B., Kushner, M.J., Rood, M.J. "Gas-Phase Removal of NO from Gas Streams via Dielectric Barrier Discharges," Environmental Science & Technology. Vol. 26, No. 4, 777-781, 1992.

Christensen, M. Personal communication with researcher. Southeast Community College Automotive Technology Department, Milford, Nebraska, 1997.

Coffman, J.A. and Browne, W.R. "Corona Chemistry," Scientific American Journal. Vol. 212, No. 6, 91-98, 1965.

Comello, V. "Reducing Auto Emissions to Ultralow Levels," R & D Magazine, p. 21, March 1996.

Desai, V.R. Decomposition of Hydrogen Sulfide in an Alternating Current, Frequency Tuned Plasma Reactor. Thesis, Oklahoma State University, 1990.

Falk, M. Research notes, NO_x destruction, Oklahoma State University, 1994.

Fujii, K., Higashi, M., Suzuki, N. "Simultaneous Removal of NO_x, CO_x, SO_x and Soot in Diesel Engine Exhaust," Non-Thermal Plasma Techniques for Pollution Control. Springer-Verlag, Berlin, 1993.

Gedra T. Personal communication with researcher. School of Electrical and Computer Engineering, Oklahoma State University, 1997.

Glockler G. and Lind, S.C. The Electrochemistry of Gases and Other Dielectrics. John Wiley and Sons, Inc., New York, 1939.

Graham, T.K. Destruction of Ethylene in a Liquid Electrode Plasma Reactor. Thesis, Oklahoma State University, 1997.

Krishnamoorthy, A. Evaluation of Dielectric Materials for Ozone Generation in Plasma Reactors. Thesis, Oklahoma State University, 1996.

Manning, D.K. Hydrocarbon Rearrangements and Synthesis Using an Alternating Current Silent Glow Discharge Reactor. Thesis, Oklahoma State University, 1993.

McCabe, W.L. and Smith, J.C. Unit Operations of Chemical Engineering. Third Edition, McGraw-Hill, New York, 1976.

McTaggart, F.K. Plasma Chemistry in Electrical Discharges. Elsevier Publishing Company, Amsterdam, 1967.

Munson, B.R., Young, D.F., Okiishi, T.H. Fundamentals of Fluid Mechanics. Second Edition, John Wiley & Sons, New York, 1994.

NASA (National Aeronautics and Space Administration) Electrical Properties of Teflon and Ceramic Capacitors at High Temperatures. NASA Technical Memorandum 105569, 1992.

Neidorf, R. "Plasma Technology Destroys VOC's, Show Promise in the Field," Environmental Information Digest, June 1996.

Newbold, R.M. Apparatus for Removing Air Pollutants from the Exhaust Stream of a Combustion Process. United State Patent #3620008, November 16, 1971.

Parker, G.W. Conceptual Design of an Industrially Applicable Plasma Reactor. Thesis, Oklahoma State University, 1993.

Patterson, D.J. and Henein, N.A. Emissions from Combustion Engines and Their Control. Ann Arbor Science Publishers, Ann Arbor, 1972.

Penetrante, B.M. and Schultheis, S.E. Non-Thermal Plasma Techniques for Pollution Control. (Introduction), Springer-Verlag, Berlin, 1993.

Piatt, M.A. Methane Destruction in an Alternating Current Plasma Reactor. Thesis, Oklahoma State University, 1988.

Rich, S.R. Exhaust Treatment System and Method. United States Patent #5284556, February 8, 1994.

Rich, S.R., Kaplan, A., Manning, M.P. Exhaust Treatment System and Method. United States Patent #5433832, July 18, 1995.

Robinowitz, S.B. Production of NOx in an Alternating Current Plasma Reactor. Thesis, Oklahoma State University, 1992.

Rosocha, L.A., Anderson, G.K., Bechtold, L.A., Coogan, J.J. Heck, H.G., Kang, M., McCulla W.H., Tennant, R.A., Wantuck, P.J. "Treatment of Hazardous Organic Wastes Using Silent Discharge Plasmas," Non-Thermal Plasma Techniques for Pollution Control., Springer-Verlag, Berlin, 1993.

Rosocha, L. and Cournoyer, M. "Nonthermal Plasma Treatment of Hazardous/Toxic Pollutants," Los Alamos National Laboratory Report (LALP-94-237). 1994.

Shäfer, F. and van Basshuysen, R. Reduced Emissions and Fuel Consumption in Automobile Engines. SAE Report, Springer-Verlag, New York, 1995.

Serway, R.A. Physics for Scientists & Engineers. Third Edition, Saunders College Publishing, Philadelphia, 1990.

Sidhu, G.S. Production and Destruction of Nitrogen Oxides in Alternating Current Plasma Reactors. Thesis, Oklahoma State University, 1995.

Simpson, R.E. Introductory Electronics for Scientists and Engineers. Second Edition, Allyn and Bacon, Inc., Boston, 1987.

Society of Automotive Engineers (SAE). "Measurement of Carbon Dioxide, Carbon Monoxide, and Oxides of Nitrogen in Automobile Exhaust," SAE J177, June 1995.

Specht, C.A. Treatment of Exhaust Gases. United States Patent #3188167, June 8, 1965.

Tsai, V. Conceptual Design and Performance Analysis of Frequency-Tuned Capacitive Discharge Reactors. Thesis, Oklahoma State University, 1991.

United States Environmental Protection Agency (EPA). Criteria Pollutants. EPA Website: http://epa.gov/docs/reg5oair/emission/critpllt.htm, 1990.

United States Environmental Protection Agency (EPA). Annual Emissions and Fuel Consumption for an "Average" Passenger Car. EPA document number: EPA420-F-97-037, 1997.

von Hippel, A.R. Dielectric Materials and Applications. Technology Press of M.I.T., New York, 1954.

World Almanac and Book of Facts, 1997. "U.S. Nitrogen Oxides Emissions Estimates, 1985-94," Environment, K-III Reference Corporation, 1996.

Appendix A:

Plasma Reactor Volume,

Gap Width, and

Capacitance Comparisons

Capacitance, Gap Width, and Annular Volume Comparisons				
Plasma Reactors				
		Annular	Annular	Total Theoretical
Reactor	Material	Gap (cm)	Volume (cc)	Capacitance (pF)
Tsai-A	pyrex	0.345	74.99	25.34
Tsai-B	pyrex	0.195	45.83	43.66
Tsai-C	pyrex	0.42	109.85	25.35
Tsai-D	pyrex	0.32	87.46	33.85
Robinowitz	pyrex	0.6	76.30	15.72
Sidhu	pyrex	0.5	129.35	38.22
Manning-A	quartz	0.49	89.54	26.35
Manning-B	pyrex	0.9	486.62	47.35
Manning-C	pyrex	0.9	1008.31	98.07
Manning-D	pyrex	0.9	1339.78	130.09
Manning-E	quartz	1	1455.25	112.35
Parker-A	quartz	0.9	630.19	61.28
Parker-B	quartz	0.35	39.38	23.85
Parker-C	quartz	0.35	39.38	23.85
Parker-D	pyrex	0.45	42.25	15.97
Parker-E	pyrex	0.2	25.53	43.32
Iftakar	pyrex	0.49	64.30	21.21
Hurst	pyrex	0.48	74.65	25.23
Lytle-A	teflon	0.665	62.88	9.97
Lytle-B	teflon	1.38	228.52	9.84

Appendix B:

Apparent Primary Power Plots

for Reactor A

and Reactor B

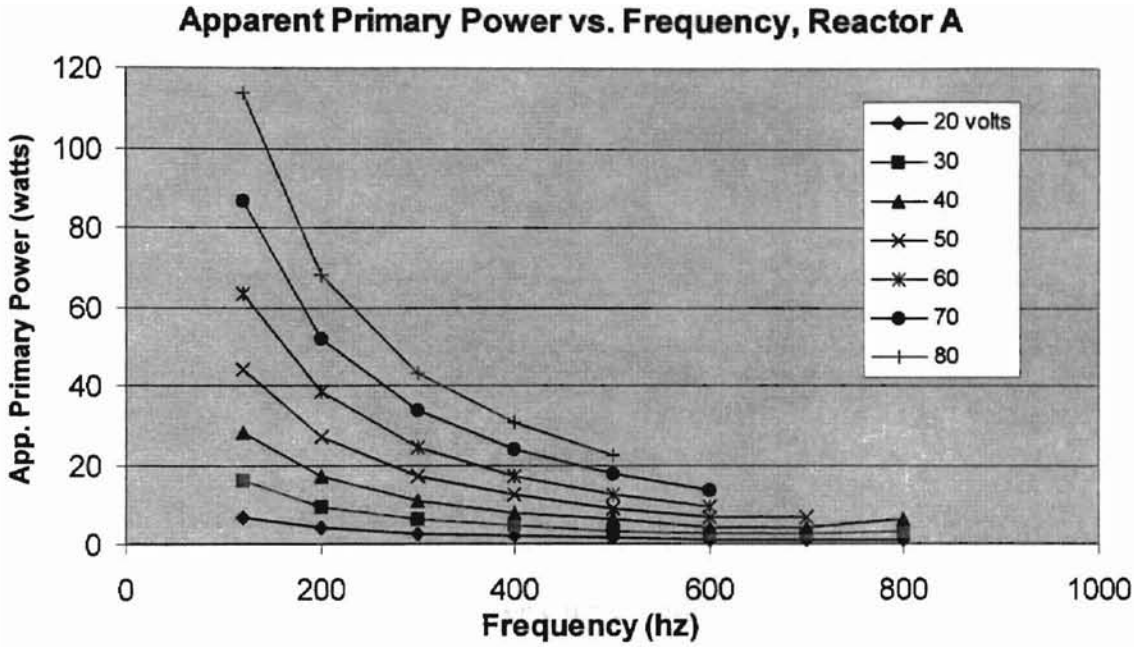
Apparent Primary Power vs. Frequency, Reactor A
App. Primary Power (watts)
120
100
80
60
40
20
0
0
200
400
600
800
1000
Frequency (hz)
20 volts
30
40
50
60
70
80

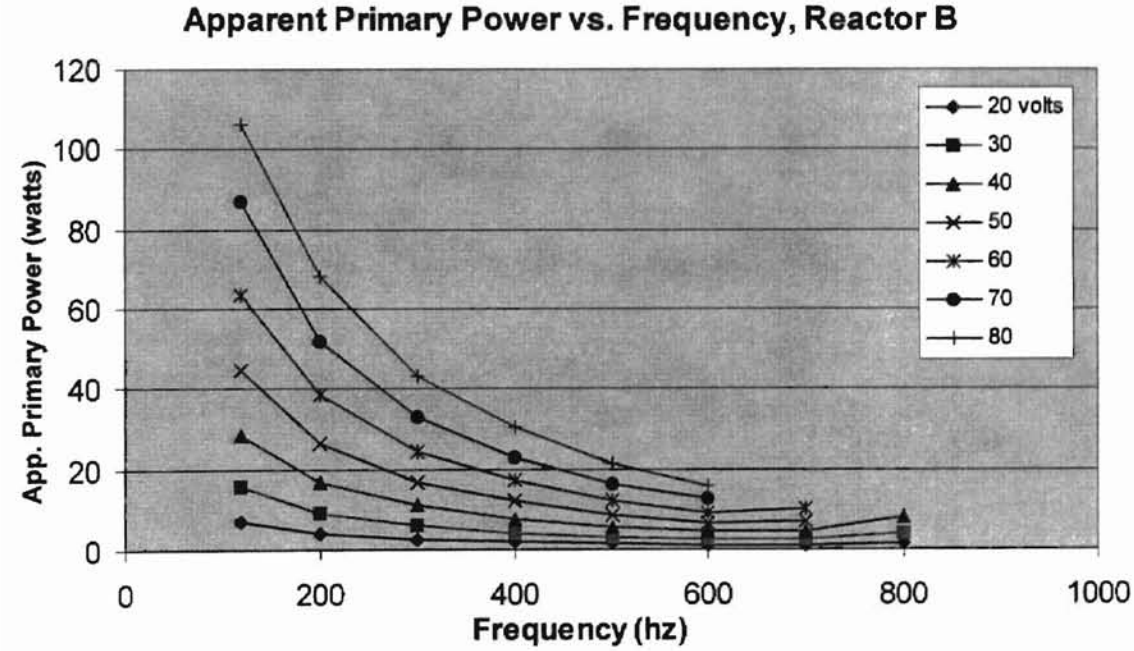
Apparent Primary Power vs. Frequency, Reactor B
App. Primary Power (watts)
120
100
80
60
40
20
0
0
200
400
600
800
1000
Frequency (hz)
20 volts
30
40
50
60
70
80

Appendix C:

Power Curve Data

Reactor A

Frequency (hz)	Vpri (volts)	Iwall (amps)	Ipri (amps)	Vsec (volts)	Vreactor (volts)	Isec (mA)
120	0	0.36	0.00	0	0	0.000
120	5	0.58	0.08	270	300	0.003
120	10	0.78	0.18	580	640	0.006
120	15	0.98	0.27	900	980	0.009
120	20	1.16	0.35	1,190	1,290	0.011
120	25	1.35	0.45	1,530	1,640	0.014
120	30	1.55	0.54	1,850	2,000	0.017
120	35	1.74	0.62	2,120	2,330	0.019
120	40	1.93	0.70	2,400	2,670	0.022
120	45	2.13	0.79	2,720	3,000	0.025
120	50	2.34	0.88	3,060	3,360	0.028
120	55	2.54	0.97	3,380	3,710	0.031
120	60	2.75	1.06	3,710	4,070	0.034
120	65	2.96	1.16	4,050	4,450	0.037
120	70	3.17	1.24	4,350	4,770	0.040
120	75	3.37	1.33	4,680	5,130	0.044
120	80	3.57	1.42	5,000	5,480	0.047
120	85	3.79	1.51	5,320	5,920	0.049
120	90	3.99	1.60	5,640	6,190	0.052
120	95	4.18	1.70	5,970	6,540	0.056
120	100	4.37	1.78	6,280	6,890	0.060
120	105	4.58	1.87	6,590	7,250	0.067
120	110	4.77	1.97	6,910	7,690	0.078
200	0	0.35	0.00	0	0	0.000
200	5	0.55	0.04	210	270	0.004
200	10	0.62	0.10	530	650	0.009
200	15	0.74	0.16	820	990	0.014
200	20	0.85	0.21	1,100	1,320	0.018
200	25	0.96	0.26	1,380	1,660	0.023
200	30	1.08	0.32	1,700	2,030	0.028
200	35	1.20	0.37	1,950	2,390	0.033
200	40	1.31	0.43	2,260	2,770	0.038
200	45	1.43	0.48	2,550	3,150	0.043
200	50	1.55	0.54	2,880	3,540	0.048
200	55	1.66	0.58	3,160	3,890	0.053
200	60	1.78	0.64	3,460	4,240	0.058
200	65	1.90	0.69	3,780	4,630	0.063
200	70	2.02	0.74	4,070	4,980	0.068
200	75	2.14	0.79	4,380	5,370	0.073
200	80	2.26	0.85	4,680	5,740	0.079
200	85	2.37	0.90	4,970	6,100	0.084
200	90	2.50	0.95	5,290	6,450	0.090
200	95	2.61	1.00	5,580	6,890	0.095
200	100	2.74	1.06	5,890	7,250	0.10
200	105	2.85	1.11	6,180	7,690	0.11
200	110					

Frequency (hz)	Vpri (volts)	Iwall (amps)	Ipri (amps)	Vsec (volts)	Vreactor (volts)	Isec (mA)
300	0	0.36	0.00	0	0	0.000
300	5	0.45	0.03	210	310	0.007
300	10	0.54	0.07	460	660	0.014
300	15	0.62	0.10	730	1,030	0.021
300	20	0.70	0.14	970	1,360	0.028
300	25	0.77	0.17	1,240	1,710	0.035
300	30	0.85	0.21	1,510	2,100	0.043
300	35	0.92	0.24	1,770	2,490	0.050
300	40	0.99	0.27	2,000	2,900	0.058
300	45	1.06	0.31	2,280	3,320	0.066
300	50	1.14	0.34	2,560	3,710	0.074
300	55	1.21	0.38	2,830	4,100	0.081
300	60	1.28	0.41	3,110	4,520	0.091
300	65	1.36	0.45	3,400	4,980	0.098
300	70	1.42	0.48	3,650	5,340	0.11
300	75	1.49	0.51	3,950	5,740	0.11
300	80	1.57	0.54	4,210	6,190	0.12
300	85	1.64	0.58	4,500	6,630	0.13
300	90	1.71	0.61	4,770	7,070	0.14
300	95	1.78	0.64	5,050	7,340	0.14
300	100	1.85	0.67	5,320	7,950	0.15
300	105					
300	110					
400	0	0.37	0.00	0	0	0.000
400	5	0.43	0.02	170	280	0.010
400	10	0.49	0.05	420	660	0.021
400	15	0.55	0.07	650	1,030	0.032
400	20	0.60	0.10	870	1,390	0.042
400	25	0.66	0.12	1,100	1,750	0.053
400	30	0.71	0.15	1,350	2,160	0.065
400	35	0.76	0.17	1,590	2,550	0.077
400	40	0.82	0.20	1,860	3,000	0.091
400	45	0.87	0.22	2,070	3,390	0.10
400	50	0.93	0.25	2,320	3,780	0.11
400	55	0.98	0.27	2,570	4,210	0.13
400	60	1.04	0.29	2,840	4,630	0.14
400	65	1.08	0.32	3,090	5,060	0.15
400	70	1.13	0.34	3,350	5,480	0.16
400	75	1.18	0.36	3,590	5,920	0.18
400	80	1.23	0.38	3,870	6,270	0.19
400	85	1.27	0.41	4,120	6,720	0.20
400	90	1.32	0.43	4,380	7,160	0.22
400	95	1.37	0.45	4,630	7,600	0.23
400	100					
400	105					
400	110					

Frequency (hz)	Vpri (volts)	Iwall (amps)	Ipri (amps)	Vsec (volts)	Vreactor (volts)	Isec (mA)
500	0	0.35	0.00	0	0	0.000
500	5	0.41	0.01	160	300	0.012
500	10	0.46	0.03	370	710	0.027
500	15	0.51	0.05	590	1,140	0.043
500	20	0.55	0.07	800	1,540	0.057
500	25	0.60	0.09	1,020	1,960	0.082
500	30	0.64	0.11	1,260	2,400	0.090
500	35	0.67	0.13	1,500	2,900	0.11
500	40	0.71	0.15	1,740	3,360	0.12
500	45	0.75	0.16	1,950	3,820	0.14
500	50	0.79	0.18	2,090	4,280	0.16
500	55	0.83	0.20	2,430	4,770	0.17
500	60	0.87	0.21	2,670	5,230	0.19
500	65	0.90	0.23	2,930	5,740	0.21
500	70	0.96	0.25	3,160	6,190	0.23
500	75	0.97	0.26	3,410	6,630	0.25
500	80	1.00	0.28	3,670	7,160	0.27
500	85	1.03	0.29	3,900	7,600	0.29
500	90					
500	95					
500	100					
500	105					
500	110					
600	0	0.35	0.00	0	0	0.000
600	5	0.40	0.01	140	310	0.015
600	10	0.44	0.02	350	810	0.036
600	15	0.48	0.04	570	1,310	0.058
600	20	0.51	0.05	770	1,750	0.078
600	25	0.54	0.07	980	2,240	0.099
600	30	0.58	0.08	1,220	2,790	0.12
600	35	0.61	0.10	1,460	3,320	0.15
600	40	0.64	0.11	1,710	3,920	0.17
600	45	0.67	0.13	1,970	4,490	0.20
600	50	0.70	0.14	2,170	5,060	0.22
600	55	0.72	0.15	2,400	5,620	0.25
600	60	0.75	0.16	2,650	6,270	0.27
600	65	0.78	0.17	2,910	6,800	0.30
600	70	0.81	0.19	3,170	7,340	0.32
600	75					
600	80					
600	85					
600	90					
600	95					
600	100					
600	105					
600	110					

Frequency (hz)	V_{prl} (volts)	I_{wall} (amps)	I_{prl} (amps)	V_{sec} (volts)	$V_{reactor}$ (volts)	I_{sec} (mA)
700	0	0.35	0.00	0	0	0.000
700	5	0.39	0.01	150	410	0.021
700	10	0.43	0.02	360	960	0.049
700	15	0.47	0.03	580	1,570	0.080
700	20	0.50	0.05	780	2,160	0.11
700	25	0.53	0.06	1,050	2,770	0.14
700	30	0.56	0.08	1,320	3,540	0.18
700	35	0.60	0.09	1,560	4,210	0.21
700	40	0.63	0.10	1,850	4,950	0.25
700	45	0.66	0.12	2,090	5,740	0.29
700	50	0.69	0.13	2,380	6,540	0.34
700	55	0.72	0.14	2,650	7,250	0.38
700	60					
700	65					
700	70					
700	75					
700	80					
700	85					
700	90					
700	95					
700	100					
700	105					
700	110					
800	0	0.35	0.00	0	0	0.000
800	5	0.39	0.01	150	480	0.028
800	10	0.44	0.02	400	1,230	0.072
800	15	0.48	0.04	650	2,030	0.12
800	20	0.53	0.06	910	2,710	0.16
800	25	0.58	0.08	1,200	3,700	0.21
800	30	0.63	0.10	1,530	4,700	0.27
800	35	0.67	0.13	1,860	5,740	0.34
800	40	0.75	0.16	2,190	6,890	0.41
800	45					
800	50					
800	55					
800	60					
800	65					
800	70					
800	75					
800	80					
800	85					
800	90					
800	95					
800	100					
800	105					
800	110					

Reactor B

Frequency (hz)	V_{prl} (volts)	I_{wall} (amps)	I_{prl} (amps)	V_{sec} (volts)	$V_{reactor}$ (volts)	I_{sec} (mA)
120	0	1.02	0.00	0	0	0.000
120	5	0.79	0.08	260	280	0.004
120	10	0.77	0.17	580	640	0.009
120	15	0.97	0.27	910	990	0.014
120	20	1.14	0.35	1,200	1,340	0.017
120	25	1.33	0.44	1,510	1,640	0.022
120	30	1.52	0.52	1,830	1,980	0.026
120	35	1.72	0.61	2,100	2,330	0.031
120	40	1.92	0.71	2,440	2,720	0.035
120	45	2.14	0.80	2,780	3,110	0.038
120	50	2.35	0.89	3,120	3,450	0.043
120	55	2.54	0.98	3,410	3,820	0.046
120	60	2.74	1.06	3,740	4,170	0.052
120	65	2.95	1.16	4,070	4,520	0.056
120	70	3.16	1.24	4,390	4,840	0.060
120	75	3.35	1.33	4,700	5,230	0.065
120	80	3.58	1.42	5,030	5,550	0.069
120	85	3.78	1.51	5,360	6,010	0.074
120	90	3.97	1.59	5,660	6,360	0.078
120	95	4.16	1.69	6,000	6,720	0.083
120	100	4.36	1.78	5,300	7,070	0.086
120	105	4.56	1.87	6,620	7,420	
120	110	4.75	1.96	6,920	7,870	
200	0	0.38	0.00	0	0	0.000
200	5	0.49	0.04	240	300	0.006
200	10	0.61	0.10	540	680	0.014
200	15	0.74	0.16	850	1,030	0.022
200	20	0.84	0.21	1,110	1,340	0.028
200	25	0.96	0.26	1,400	1,670	0.034
200	30	1.07	0.31	1,700	2,070	0.042
200	35	1.19	0.37	1,970	2,470	0.049
200	40	1.31	0.42	2,280	2,830	0.056
200	45	1.42	0.48	2,580	3,180	0.064
200	50	1.54	0.53	2,900	3,610	0.072
200	55	1.66	0.59	3,200	3,960	0.079
200	60	1.77	0.64	3,500	4,380	0.087
200	65	1.90	0.69	3,820	4,700	0.094
200	70	2.01	0.74	4,120	5,090	0.10
200	75	2.13	0.80	4,420	5,440	0.11
200	80	2.25	0.85	4,740	6,010	0.12
200	85	2.38	0.90	5,020	6,360	0.12
200	90	2.48	0.95	5,310	6,630	0.13
200	95	2.60	1.00	5,610	7,070	0.14
200	100	2.72	1.05	5,920	7,420	0.15
200	105	2.83	1.10	6,200	7,780	0.15
200	110	2.94	1.15	6,490	8,130	0.16

Frequency (hz)	V_{prl} (volts)	I_{wall} (amps)	I_{prl} (amps)	V_{sec} (volts)	$V_{reactor}$ (volts)	I_{sec} (mA)
300	0	0.43	0.00	0	0	0.000
300	5	0.47	0.03	200	300	0.011
300	10	0.53	0.06	470	680	0.022
300	15	0.61	0.10	760	1,080	0.034
300	20	0.68	0.13	990	1,410	0.044
300	25	0.76	0.17	1,260	1,800	0.055
300	30	0.83	0.20	1,530	2,190	0.068
300	35	0.91	0.24	1,820	2,580	0.081
300	40	0.99	0.28	2,070	3,000	0.093
300	45	1.06	0.31	2,350	3,390	0.11
300	50	1.13	0.34	2,620	3,820	0.12
300	55	1.20	0.38	2,890	4,240	0.13
300	60	1.27	0.41	3,160	4,670	0.14
300	65	1.35	0.44	3,450	5,090	0.16
300	70	1.41	0.47	3,700	5,410	0.16
300	75	1.49	0.50	3,980	6,010	0.18
300	80	1.56	0.54	4,250	6,360	0.19
300	85	1.63	0.57	4,550	6,720	0.20
300	90	1.70	0.60	4,840	7,160	0.22
300	95	1.77	0.63	5,070	7,510	0.23
300	100	1.84	0.67	5,370	8,040	0.24
300	105	1.92	0.70	5,640	8,480	0.25
300	110	1.98	0.73	5,900	8,840	0.27
400	0	0.37	0.00	0	0	0.000
400	5	0.42	0.02	180	280	0.015
400	10	0.49	0.05	440	710	0.033
400	15	0.55	0.07	660	1,060	0.048
400	20	0.60	0.10	890	1,430	0.065
400	25	0.66	0.12	1,130	1,840	0.081
400	30	0.71	0.14	1,390	2,230	0.099
400	35	0.77	0.17	1,660	2,650	0.12
400	40	0.82	0.19	1,920	3,110	0.14
400	45	0.87	0.22	2,120	3,540	0.16
400	50	0.92	0.24	2,400	3,960	0.17
400	55	0.97	0.26	2,650	4,350	0.19
400	60	1.02	0.29	2,910	4,770	0.21
400	65	1.07	0.31	3,180	5,060	0.23
400	70	1.11	0.33	3,420	5,590	0.25
400	75	1.16	0.35	3,690	6,190	0.27
400	80	1.21	0.38	3,960	6,540	0.29
400	85	1.26	0.40	4,230	6,980	0.31
400	90	1.31	0.42	4,490	7,340	0.33
400	95	1.35	0.44	4,750	7,780	0.34
400	100	1.39	0.46	5,020	8,220	0.36
400	105	1.44	0.48	5,280	8,660	0.38
400	110	1.49	0.50	5,540	9,100	0.40

Frequency (hz)	Vpri (volts)	Iwall (amps)	Ipri (amps)	Vsec (volts)	Vreactor (volts)	Isec (mA)
500	0	0.36	0.00	0	0	0.000
500	5	0.40	0.01	150	280	0.016
500	10	0.46	0.03	380	730	0.041
500	15	0.50	0.05	630	1,190	0.067
500	20	0.54	0.07	840	1,610	0.081
500	25	0.58	0.08	1,080	2,050	0.11
500	30	0.62	0.10	1,330	2,530	0.14
500	35	0.66	0.12	1,570	3,000	0.16
500	40	0.70	0.14	1,830	3,500	0.19
500	45	0.74	0.15	2,050	3,990	0.22
500	50	0.77	0.17	2,300	4,490	0.24
500	55	0.81	0.19	2,550	4,950	0.27
500	60	0.84	0.20	2,810	5,440	0.29
500	65	0.88	0.22	3,090	6,010	0.33
500	70	0.91	0.23	3,320	6,500	0.35
500	75	0.95	0.25	3,610	6,980	0.38
500	80	0.98	0.27	3,850	7,420	0.41
500	85	1.01	0.28	4,110	7,950	0.43
500	90	1.05	0.30	4,380	8,400	0.46
500	95	1.08	0.31	4,640	9,010	0.48
500	100	1.11	0.33	4,900	9,460	0.51
500	105					
500	110					
600	0	0.36	0.00	0	0	0.000
600	5	0.39	0.01	160	360	0.024
600	10	0.44	0.02	390	890	0.058
600	15	0.48	0.04	640	1,470	0.094
600	20	0.51	0.05	850	1,910	0.12
600	25	0.54	0.06	1,090	2,420	0.16
600	30	0.57	0.08	1,330	2,970	0.19
600	35	0.60	0.09	1,600	3,570	0.23
600	40	0.63	0.11	1,880	4,170	0.27
600	45	0.66	0.12	2,100	4,770	0.31
600	50	0.69	0.13	2,370	5,410	0.35
600	55	0.71	0.14	2,650	6,100	0.37
600	60	0.74	0.15	2,920	6,630	0.43
600	65	0.77	0.17	3,210	7,340	0.47
600	70	0.79	0.18	3,480	7,870	0.51
600	75	0.82	0.19	3,740	8,480	0.55
600	80	0.84	0.20	4,030	9,100	0.59
600	85	0.86	0.21	4,320	9,720	0.64
600	90					
600	95					
600	100					
600	105					
600	110					

Frequency (hz)	V_{prl} (volts)	I_{wall} (amps)	I_{prl} (amps)	V_{sec} (volts)	$V_{reactor}$ (volts)	I_{sec} (mA)
700	0	0.37	0.00	0	0	0.000
700	5	0.40	0.01	170	450	0.034
700	10	0.44	0.02	410	1,040	0.079
700	15	0.47	0.04	480	1,770	0.13
700	20	0.51	0.05	920	2,370	0.18
700	25	0.54	0.06	1,210	3,150	0.23
700	30	0.58	0.08	1,500	3,850	0.29
700	35	0.61	0.09	1,800	4,670	0.35
700	40	0.64	0.11	2,060	5,440	0.41
700	45	0.68	0.12	2,410	6,360	0.47
700	50	0.72	0.14	2,750	7,250	0.54
700	55	0.75	0.16	3,060	8,040	0.60
700	60	0.79	0.17	3,400	8,840	0.67
700	65	0.82	0.19	3,750	9,810	0.73
700	70					
700	75					
700	80					
700	85					
700	90					
700	95					
700	100					
700	105					
700	110					
800	0	0.36	0.00	0	0	0.000
800	5	0.39	0.01	160	570	0.049
800	10	0.45	0.02	460	1,340	0.11
800	15	0.51	0.05	790	2,300	0.23
800	20	0.56	0.07	1,120	3,290	0.27
800	25	0.63	0.10	1,490	4,310	0.37
800	30	0.69	0.13	1,870	5,410	0.46
800	35	0.77	0.16	2,270	6,720	0.57
800	40	0.85	0.20	2,720	7,950	0.68
800	45	0.94	0.24	3,210	9,370	0.80
800	50					
800	55					
800	60					
800	65					
800	70					
800	75					
800	80					
800	85					
800	90					
800	95					
800	100					
800	105					
800	110					

Frequency (hz)	Vpri (volts)	Iwall (amps)	Ipri (amps)	Vreactor (volts)	Isec (mA)
400	0	0.37	0	0	0
400	5	0.42	0.01	250	0.028
400	10	0.49	0.04	680	0.067
400	15	0.55	0.07	1150	0.11
400	20	0.61	0.09	1540	0.14
400	25	0.66	0.11	1930	0.18
400	30	0.71	0.14	2370	0.22
400	35	0.76	0.16	2760	0.26
400	40	0.81	0.19	3220	0.3
400	45	0.86	0.21	3680	0.34
400	50	0.91	0.23	4140	0.39
400	55	0.96	0.26	4560	0.42
400	60	1.01	0.28	5020	0.47
400	65	1.06	0.3	5570	0.49
400	70	1.1	0.32	5920	0.57
400	75	1.15	0.34	6450	0.6
400	80	1.2	0.37	6850	0.64
400	85	1.24	0.39	7250	0.68
400	90	1.29	0.41	7780	0.72
400	95	1.33	0.43	8130	0.77
400	100	1.37	0.45	8570	0.8
200	70	1.99	0.74	5200	0.21
250	70	1.65	0.58	5480	0.27
300	70	1.42	0.47	5570	0.39
350	70	1.24	0.39	5660	0.47
400	70	1.1	0.32	5920	0.57
450	70	0.98	0.26	6270	0.66
500	70	0.89	0.22	6980	0.81
550	70	0.81	0.19	7870	1.34
600	70	0.81	0.18	9100	1.29

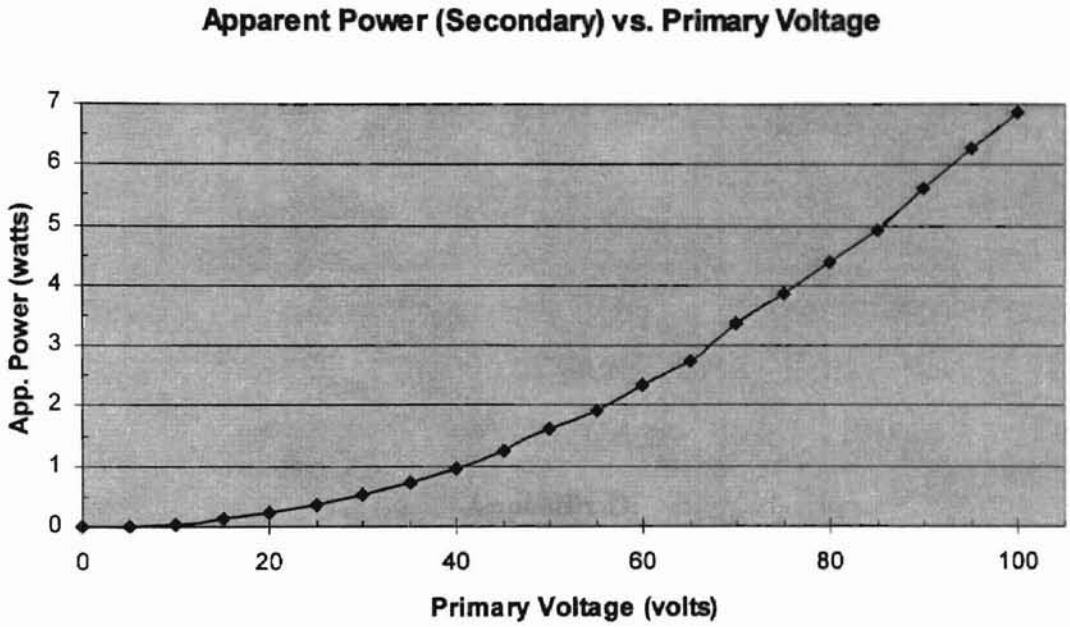
Apparent Power (Secondary) vs. Primary Voltage
App. Power (watts)
0
1
2
3
4
5
6
7
0
20
40
60
80
100
Primary Voltage (volts)

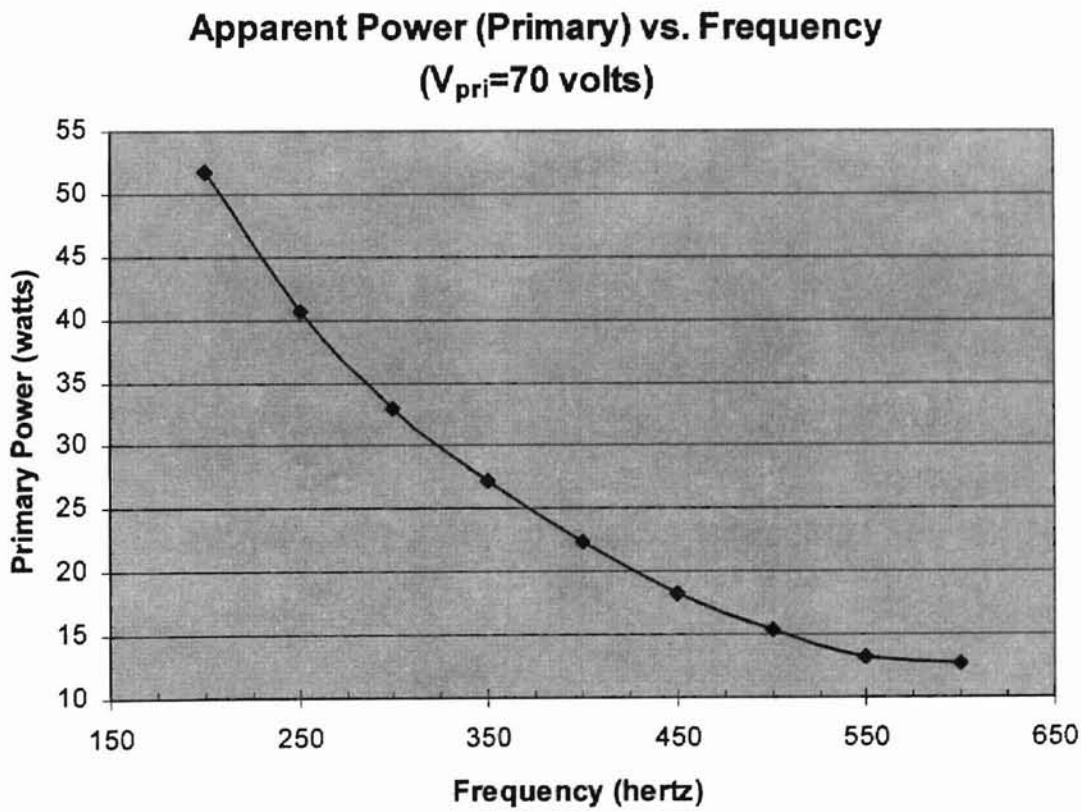
Apparent Power (Primary) vs. Frequency
(V_{pri}=70 volts)
Primary Power (watts)
10
15
20
25
30
35
40
45
50
55
150
250
350
450
550
650
Frequency (hertz)

Appendix D:

Reynolds Number Calculations

Reynolds Number Calculations		
D_o=	0.0174	meters
D_i=	0.0041	meters
μ=	1.79E-05	N*sec/m^2
ρ=	1.23	kg/m^3
V=	0.0000629	m^3
Residence	Flowrate	Reynolds
Time (sec)	(m^3/sec)	Number (-)
1.0	6.29E-05	414
2.5	2.52E-05	166
5.0	1.26E-05	83

Appendix E:

Destruction Efficiency Data

Destruction Runs
(θ=5 seconds, f=400 hertz)
(V_{sec}=10,500 volts)

Humidity									
26% Humidity			40%				80%		
Co (ppm)	Ce (ppm)	D.E. (%)	Co (ppm)	Ce (ppm)	D.E. (%)	3*St Dev.	Co (ppm)	Ce (ppm)	D.E. (%)
50	52	-4.0	46	9	82.3	5.47	50	11	78.0
96	86	10.4	99	12	87.9		97	13	86.6
190	160	15.8	200	18.5	94.2	1.55	200	24	88.0
420	385	8.3	400	160	60.0		425	45	89.4
820	810	1.2	800	645	16.3	1.42	805	640	20.5
1550	1540	0.6	1500	1390	7.3		1500	1390	7.3
2100	2100	0.0	2010	1920	4.5		2000	1920	4.0

40%, Co=50 ppm		
Co	Ce	D.E. (%)
48	9.5	80.21
47	9.2	80.43
49	8.2	83.27
49	7.7	84.29
46	7.8	83.04
	Average:	82.25
	St. Dev:	1.82357
	St. Dev*3:	5.4707

40%, Co=190 ppm		
Co	Ce	D.E. (%)
200	12.5	93.75
205	11.5	94.39
205	10.5	94.88
200	11	94.50
205	13	93.66
	Average:	94.24
	St. Dev:	0.5185
	St. Dev*3:	1.5555

40%, Co=820 ppm		
Co	Ce	D.E. (%)
820	685	16.46
830	690	16.87
830	695	16.27
835	700	16.17
835	705	15.57
	Average:	16.27
	St. Dev:	0.47339
	St. Dev*3:	1.42018

Destruction Runs Examining Reactor Voltage
(θ=5 seconds, f=400 hertz)
(C=200 ppm)

	25% (Low Humidity)			40% (Mid Humidity)			85% (High Humidity)		
Reactor Voltage (volts)	Co (ppm)	Ce (ppm)	Dest. Eff. (%)	Co (ppm)	Ce (ppm)	Dest. Eff. (%)	Co (ppm)	Ce (ppm)	Dest. Eff. (%)
8000				200	180	10.0	198	180	9.1
8500	198	196	1.0	200	163	18.5	195	135	30.8
9000	205	160	22.0	200	150	25.0	200	125	37.5
9500	205	145	29.3	202	125	38.1	200	110	45.0
10000	205	142	30.7	205	17.5	91.5	200	22	89.0
10500	208	145	30.3	200	13.5	93.3	200	16	92.0
11000	205	145	29.3	202	14	93.1	202	19	90.6

Destruction Runs Examining Residence Time & Frequency
(V_{sec}=10,000 volts, Humidity=40%)
(C=200 ppm)

	Residence Time								
	5 sec			2.5			1.0		
Frequency (hz)	Co (ppm)	Ce (ppm)	D.E. (%)	Co (ppm)	Ce (ppm)	D.E. (%)	Co (ppm)	Ce (ppm)	D.E. (%)
60	205	81	60.5	201	122	39.3	202	168	16.8
200	200	19.5	90.3	200	54	73.0	201	114	43.3
300	200	17	91.5	200	42	79.0	202	69	65.8
400	200	16.2	91.9	198	41	79.3	200	54	73.0
500	200	17	91.5	203	44	78.3	200	50	75.0
600	200	24	88.0	207	50	75.8	200	51	74.5

Cyclical Residence Time (cycles)	Destruction Efficiency (%)	Standard Deviation (%)
60	16.8	
150	39.3	
200	43.3	
300	63.2	
400	73	
500	74	5.18
600	74.5	
750	79	
1000	84.38	3.48
1250	78.3	
1500	87.06	3.57
2000	91.9	
2500	91.5	
3000	88	

Repeat Runs

500 cycles

Co	Ce	Dest Eff (%)
205	82	60.00
207	88	57.49
203	83	59.11
208	103	50.48
197	100	49.24
200	102	49.00
	Average:	54.22
St. Deviation:		5.18

1000 cycles

Co	Ce	Dest Eff (%)
215	27	87.44
207	23	88.89
207	29	85.99
202	37	81.68
200	38	81.00
203	38	81.28
	Average:	84.38
St. Deviation:		3.48

1500 cycles

Co	Ce	Dest Eff (%)
202	20	90.10
196	18.5	90.56
204	20	90.20
204	34	83.33
200	33	83.50
202	31	84.65
	Average:	87.06
St. Deviation:		3.57

Destruction Run Examining Reproducibility

(V_{sec}=10,000 volts, Humidity=40%)

(C=200 ppm, θ=2.5 seconds)

Trial #	Co (ppm)	Ce (ppm)	Destruction Efficiency (%)
1	199	97	51.3
2	202	98	51.5
3	205	100	51.2
4	212	108	49.1
5	198	97	51.0
6	215	105	51.2
7	203	97	52.2
8	202	97	52.0
		Mean	51.2
	Standard Deviation		0.953

Appendix F:

Ozone Titration Data

Ozone Production Results						
(Co=200 ppm=0.26 mg/L)						
(Humidity=40%)						
Normality of $Na_2S_2O_3$:		0.05	N			
Frequency	Residence	Corresponding	Elapsed	Titrant	Ozone	Ozone Production Rate
(hertz)	Time (sec)	Flowrate (ml/min)	Time (min)	Used (ml)	Conc. (mg/L)	(mg O_3/mg NO_x removed)
300	1	3770	9	16	0.57	3.30
300	1	3770	8.5	14.4	0.54	3.14
				Average	**0.55**	**3.22**
300	5	755	17.5	6.4	0.58	2.43
300	5	755	19	7.2	0.60	2.52
				Average	**0.59**	**2.47**
400	1	3770	7	12.4	0.56	2.97
400	1	3770	6.5	10.8	0.53	2.79
				Average	**0.55**	**2.88**

VITA

Patrick H. Lytle

Candidate for the Degree of Master of Science

Thesis: DESTRUCTION OF NITROGEN OXIDES USING A DIELECTRIC BARRIER DISCHARGE PLASMA REACTOR

Major Field: Environmental Engineering

Personal Data: Born in Beatrice, Nebraska, September 15, 1972; Raised in Odell, Nebraska; the son of Carl and Marilyn Lytle

Education: Graduated from Odell High School in May 1991

Bachelor of Arts Degree in Physics and Music, from Hastings College; Hastings, Nebraska in May 1996

Completed the requirements for the Master of Science degree with a major in Environmental Engineering at Oklahoma State University in May 1998

Experience: Employed by Davis Land Surveying as *CADD Draftsman/Crew Chief* from May 1993 to August 1996

Worked for Oklahoma State University as *Graduate Teaching/Lab Assistant* from August 1996 to May 1998

Served as *Engineering Intern* for Montgomery Watson (Tulsa, Oklahoma office) the summer of 1997

Professional Memberships: American Society of Civil Engineers
Phi Mu Alpha Sinfonia
Chi Epsilon Engineering Honor Society
Alpha Chi Scholastic Honorary
Phi Kappa Phi